Science of the Total Environment 926 (2024) 171751

Contents lists available at ScienceDirect

Science of the Total Environment

journal homepage: www.elsevier.com/locate/scitotenv

# Unravelling the main mechanism responsible for nocturnal $CO_2$ uptake by dryland soils

Minsu Kim [a,*,1], Clément Lopez-Canfin [b,c,1], Roberto Lázaro [d], Enrique P. Sánchez-Cañete [b,e], Bettina Weber [a,f]

[a] Institute of Biology, University of Graz, Graz, Austria
[b] Department of Applied Physics, University of Granada (UGR), Granada, Spain
[c] Department of Plant and Soil Sciences, University of Delaware, Newark, DE, USA
[d] Department of Desertification and Geo-Ecology, Experimental Station of Arid Zones (EEZA-CSIC), Almería, Spain
[e] Inter-University Institute for Earth System Research (IISTA-CEAMA), Granada, Spain
[f] Multiphase Chemistry, Max Planck Institute for Chemistry, Mainz, Germany

## HIGHLIGHTS

- Nocturnal $CO_2$ uptake by dryland soils is explained with a mechanistic model.
- Diel temperature cycles were the main driver by increasing $CO_2$ solubility at night.
- Alkalization of thin soil water films at night can induce carbonate precipitation.
- Biological soil crusts have the potential to modulate the abiotic $CO_2$ uptake.
- These mechanisms can contribute to the global residual terrestrial carbon sink.

## GRAPHICAL ABSTRACT

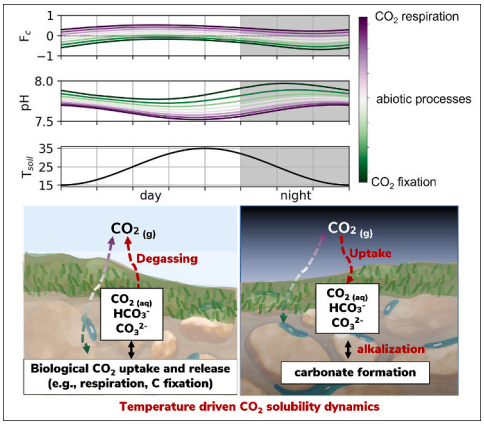


## ARTICLE INFO

Editor: Wei Shi

## ABSTRACT

Soil respiration, or $CO_2$ efflux from soil, is a crucial component of the terrestrial carbon cycle in climate models. Contrastingly, many dryland soils absorb atmospheric $CO_2$ at night, but the exact mechanisms driving this uptake are actively debated. Here we used a mechanistic model with heuristic approaches to unravel the underlying processes of the observed patterns of soil-atmosphere $CO_2$ fluxes. We show that the temperature drop during nighttime is the main driver of $CO_2$ uptake by increasing $CO_2$ solubility and local water pH of a thin water film on soil particle surfaces, providing favourable conditions for carbonate precipitation. Our data demonstrate that the nocturnal inorganic carbon absorption is a common soil process, but often offset by biological $CO_2$ production. The uptake rates can be impacted by different successional stages of biocrusts that consume or produce $CO_2$ and

* Corresponding author.
*E-mail address:* minsu.kim@uni-graz.at (M. Kim).
[1] These authors contributed equally

https://doi.org/10.1016/j.scitotenv.2024.171751
Received 17 November 2023; Received in revised form 21 February 2024; Accepted 14 March 2024
Available online 17 March 2024

modify the pH of the soil water film, which can be maintained by non-rainfall water inputs, such as pore space condensation. Annual estimates of nocturnal carbon uptake, based on in situ continuous measurements at the soil level in drylands are still very scarce, but fluxes of up to several tens of g C $m^{-2}$ $y^{-1}$ have been reported, potentially accounting for a considerable fraction of the global residual terrestrial carbon sink.

## 1. Introduction

Soils are a major reservoir of carbon (C), storing organic C (1530 Pg), solid inorganic C as mostly carbonates (940 Pg), and dissolved inorganic C in soil solution (1404 Pg) (Monger et al., 2015). Each pool amounts to more C than is contained in the vegetation (450–650 Pg) or the atmosphere (828 Pg) globally (IPCC, 2013). Soil C is continuously exchanged with the atmosphere through $CO_2$ fluxes ($F_c$) resulting from $CO_2$ production, consumption, and transport processes in soil at an estimated rate of 87 ± 9 Pg $y^{-1}$ (Jian et al., 2022). Locally, $F_c$ can be either positive ($CO_2$ efflux) or negative ($CO_2$ influx), depending on the balance between $CO_2$ production and consumption. In most environments $F_c$ has been found to be positive, and research has mainly focused on understanding $CO_2$ production through respiration of roots, microorganisms and decomposition of organic matter (Goffin et al., 2015; Jochheim et al., 2022; Lu et al., 2021; Ryan and Law, 2005; Waring and Powers, 2016).

However, dryland soils around the globe have been increasingly reported to absorb atmospheric $CO_2$ at night suggesting a possible role of soil $CO_2$ consumption processes on the C balance of water-limited ecosystems (Fa et al., 2015; Hamerlynck et al., 2013; Sagi et al., 2021; Sánchez-Cañete et al., 2018; Yates et al., 2013). Due to the large extension of drylands representing around 45 % of Earth's land surface (Lal, 2019), the observed nocturnal $CO_2$ uptake could contribute to explain the residual/missing terrestrial C sink (3.1 ± 0.9 Pg $y^{-1}$) (Houghton et al., 2018), i.e., the imbalance in the global C budget that remained unresolved for decades. On the other hand, some authors have shown skepticism regarding the relevance and significance of these fluxes at the global scale (Schlesinger, 2017; Schlesinger et al., 2009), essentially arguing that the reported rates of $CO_2$ uptake were incompatible with plausible mechanisms of $CO_2$ consumption and therefore due to inaccurate instrumentation.

Drylands offer unique conditions to study $CO_2$ consumption processes in soil. Although these processes are likely ubiquitous across ecosystems, soil $CO_2$ consumption is often masked by high respiration rates in mesic or humid environments where it can remain undetected by flux measurements. In contrast, drylands maintain low $CO_2$ production rates in soil: the scarcity of plants strongly reduces root respiration, and the decomposition of organic matter is limited by the low water availability as well as low soil organic carbon (SOC) content and SOC bounding to carbonates. With 80 to 97 % of the soil solid inorganic carbon (SIC) (mainly as $CaCO_3$) located in water-limited ecosystems, SIC stocks often largely exceed SOC stocks (Plaza et al., 2018). However, despite such favourable conditions to detect $CO_2$ consumption in drylands, the mechanisms involved in nocturnal $CO_2$ uptake remain actively debated (Sagi et al., 2021).

It is important to unravel the mechanisms of nocturnal $CO_2$ uptake by dryland soils to predict the impact of climate change on the C storage of drylands, and to explore novel strategies to mitigate climate change. Some studies have found contradictory results on this topic, for example, the observation of $CO_2$ uptake only during dry conditions (Hamerlynck et al., 2013) or only during wet conditions (Fa et al., 2015, 2016b; Yates et al., 2013). This highlights the complexity of disentangling the mechanisms involved in the $CO_2$ uptake. Mostly, the following processes have been suggested to explain this uptake: (1) pH- and temperature-driven $CO_2$ dissolution, and subsequent leaching to aquifers (Ma et al., 2013, 2014; Wang et al., 2020); (2) calcium carbonate dissolution (Fa et al., 2016a, 2016b); (3) thermal convection, diel expansion/contraction of soil air promoted by temperature changes (Gao et al., 2021; Yang et al., 2020); (4) $CO_2$ adsorption on soil particles (Davidson et al., 2013; Lopez-Canfin et al., 2022a); (5) precipitation of secondary carbonates favoured by the weathering of Ca-bearing minerals other than $CaCO_3$ (Lopez-Canfin et al., 2022b). In particular, the latter mechanism deserves special attention since it represents a long-term C sink due to the exogenic origin of Ca (Monger et al., 2015; Sanderman, 2012).

The dynamics of carbonate formation are usually considered to be slower than the nocturnal $CO_2$ uptake reported for drylands. For example, in semiarid areas, C sequestration rates through carbonate precipitation is estimated to range between 0.3 and 12.4 g C $m^{-2}$ $yr^{-1}$ (Lal, 2001) while the nocturnal $CO_2$ uptake can be slightly faster, with estimates from continuous in situ measurements at the soil level of up to several tens of g C $m^{-2}$ $yr^{-1}$ (Lopez-Canfin et al., 2022a). However, those estimates are not incompatible and remain scarce, thus uncertain at the global scale. In addition, soil microbiota could potentially accelerate this geochemical process through biomineralization (Liu et al., 2020). In drylands, biological soil crusts (hereafter biocrusts) are communities of cyanobacteria, algae, bacteria, lichens and mosses that inhabit the top few centimetres of the soil (Garcia-Pichel, 2023; Weber et al., 2022). These are hotspots of microbial activity that drive biogeochemical processes sustaining important ecological functions in drylands. Such functions include the alteration of $F_c$ (Darrouzet-Nardi et al., 2018), the modification of soil physico-chemical properties such as pH (Büdel et al., 2004; Wu et al., 2013), porosity (Miralles-Mellado et al., 2011), soil water and SOC content (Chamizo et al., 2016), as well as enhanced mineral weathering and biomineralization (Benzerara et al., 2014; Büdel et al., 2004; Chen et al., 2014; Souza-Egipsy et al., 2004). However, considering that the lack of water hinders biological activity and most soil $CO_2$ consumption processes, it is important to comprehend how these components interact during dry spells. So far, little attention has been given to abiotic $CO_2$ uptake in soils covered by biocrusts with modified physicochemical properties and predictive mechanistic or process-based models are needed to explain these field observations at the sub-diurnal resolution.

In this study, we aim at unravelling the dominant mechanism responsible for nocturnal soil $CO_2$ uptake using a mechanistic model, the simplified field application of Desert Biocrust Model (sfDBM), to simulate processes governing $F_c$. We disentangle different $CO_2$ uptake processes: (1) the dissolution of $CO_2$ driven by an increase in solubility at night; (2) the role of inorganic C partitioning that depends on soil water pH affecting inorganic C dynamics; (3) the contributions of these processes by biocrusts at different successional stages (Fig. S1). We validate our model predictions using continuous measurements of soil-atmosphere $CO_2$ fluxes and micrometeorological variables from a semiarid desert where nocturnal $CO_2$ uptake occurs on a regular basis (Lopez-Canfin et al., 2022b, 2024).

## 2. Results

### 2.1. Hourly measurements of soil-atmosphere $CO_2$ exchange and other environmental variables

The soil-atmosphere $CO_2$ exchange ($F_c$) displayed strong diel variability (coefficient of dispersion (CV) of all crusts = 135 %), which was comparable to the seasonal variability (CV = 126 %; Fig. 1a). The distribution of $F_c$ was skewed (Fisher-Pearson coefficient of skewness = 0.72) due to sporadic rainfall events that triggered enhanced $F_c$ for all crusts (Fig. S2, Fig. S3). At nighttime, atmospheric $CO_2$ uptake by soil was very frequent in early successional stages and even more frequent than $CO_2$ release ($F_c$ median = − 0.10 μmol $m^{-2}$ $s^{-1}$) (Fig. S2). By

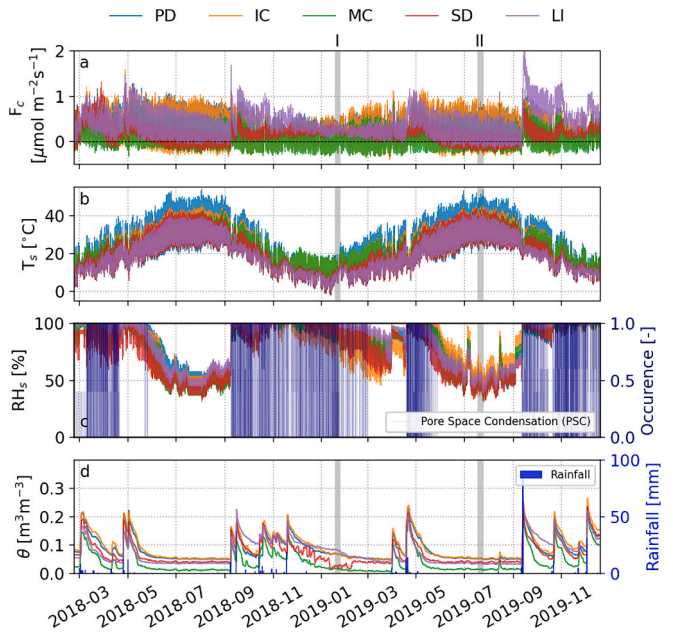


**Fig. 1.** Hourly time series of environmental measurements averaged by crust type. (a) soil-atmosphere $CO_2$ exchange ($F_c$); (b) soil temperature ($T_s$); (c) soil relative humidity ($RH_s$) and possible pore-space condensation in soil (navy bars); and (d) daily time series of soil water content (θ) and daily rainfall shown with blue bars. The time series of θ are displayed at daily resolution, instead of hourly resolution, because sensors were not accurate enough to capture the diel variability in this variable. Line colours of each panel indicate biocrust type; PD, physical depositional crust ($n$ = 3 replicates) in blue; IC, incipient cyanobacteria (n = 3) in orange; MC, mature cyanobacteria ($n$ = 5) in green; SD, lichen community dominated by *Squamarina lentigera* and *Diploschistes diacapsis* (n = 3) in red; LI, lichen community characterized by *Lepraria isidiata* (n = 3) in purple. Grey shaded areas indicate the dry periods with contrasting temperature conditions selected to test the predictions of the mechanistic model: test periods are numbered as (I) dry and cool; (II) dry and hot.

contrast, soil $CO_2$ release was more frequent than $CO_2$ uptake in late successional stages (median = 0.19 μmol $m^{-2}$ $s^{-1}$) (Fig. S2). The soil temperature ($T_s$) showed strong diel and seasonal variability, with a similar pattern across crust types but remarkably greater diel fluctuations in the physical depositional (PD) crust (Fig. 1b). The soil relative humidity ($RH_s$) and possible pore-space condensation (PSC, defined as the condition when soil temperature is equal or lower than the dew point at 5 cm depth) were substantially lower during summer than the rest of the year (Fig. 1c). The occurrence of PSC was more likely during nighttime and under wet or cool conditions (Fig. S4). The soil water content (θ) dynamics exhibited a pattern of pulses governed by rainfall events and subsequent drying (Fig. 1d).

### 2.2. Diel and seasonal patterns of $CO_2$ uptake by soil

The daily averaged time series of $CO_2$ release, uptake, and resultant net $F_c$ as well as the average diel $F_c$ cycle during contrasting periods in terms of both moisture and temperature are shown in Fig. 2. In addition, hourly time series and daily cumulative values of $F_c$ during two dry periods under contrasting temperature conditions (dry and cool - winter vs. dry and hot - summer, marked as grey shaded areas I and II in Fig. 1) are plotted in Fig. 3. Overall, $CO_2$ uptake by soil was shaped by wetness, temperature and biocrust type. Uptake was greater in early successional stages (from physical depositional to cyanobacterial crusts; PD, IC, and MC) and persisted throughout the whole study period (Fig. 2a-e). It occurred during nighttime whereas $CO_2$ release occurred during daytime (Fig. 2f-i). Overall, the $CO_2$ uptake was greater during dry periods compared to wet periods (Fig. 2f-i). Among dry periods, the daily $CO_2$

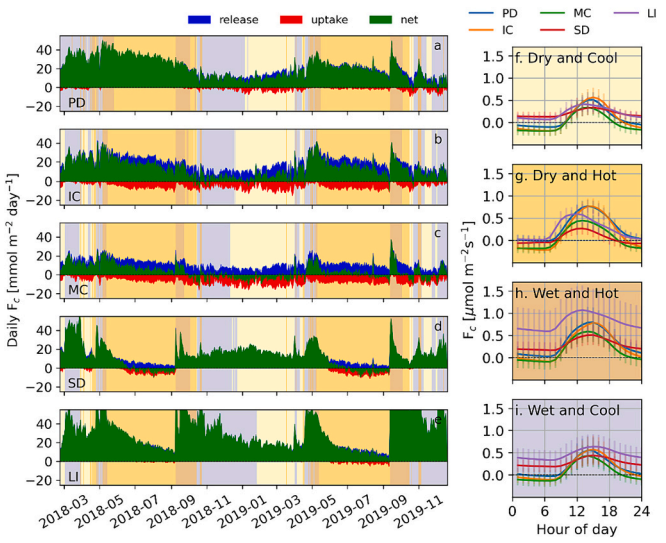


**Fig. 2.** Daily averaged time series of soil-atmosphere $CO_2$ flux ($F_c$) and diel $F_c$ patterns under contrasting climatic periods. (a-e) Daily time series of $F_c$ (averaged by biocrust type) subdivided into release (sum of positive hourly flux), uptake (sum of negative hourly flux), and net (daily sum of flux) values; (f-i) Average diel $F_c$ patterns. Values are averaged by crust type: PD, physical depositional; (b) IC, incipient cyanobacteria; (c) MC, mature cyanobacteria; (d) SD, lichen community dominated by *Squamarina lentigera* and *Diploschistes diacapsis* and (e) LI, lichen community characterized by *Lepraria isidiata*. Note that the high values of LI in (e) are truncated for comparison across crust types. Classified dry/wet, and cool/hot periods are colour-shaded as follows: dry and cool (bright yellow), dry and hot (orange), wet and hot (brown), and wet and cool (purple) (f-i) The error bars represent the hourly standard deviation.

uptake increased under hot conditions and occurred even in late succession stages (Lichen crusts: SD and LI) (Fig. 3). Daily net $CO_2$ uptake occurred mainly under dry conditions in the MC crusts during winter and in the SD crusts during summer.

### 2.3. Effect of temperature-dependent $CO_2$ solubility on carbon uptake dynamics

The effect of temperature dynamics on $F_c$ was examined with the sfDBM using a heuristic approach, representing a method of learning that uses simplified boundary conditions compared to field data. Here, to simulate the diel cycle of temperature, a sinusoidal function with a 24-h-period was used (Eq. (1)). The soil domain was set to be at a dry condition (θ ≈ 0.05 $m^3$ $m^{-3}$, effective film thickness on soil particles ≈1 $m^{-7}$). The model prediction showed a non-linear response of $F_c$ dynamics to temperature changes (Fig. 4). At lower average temperature, the amplitude of the diel $CO_2$ cycle was higher, as influenced by greater temporal changes in temperature-driven $CO_2$ solubility (Henry's law). Essentially, the $F_c$ dynamics followed the dynamics of time derivatives of temperature ($dT/dt$ in Fig. 4b), reflecting $CO_2$ dissolution and degassing caused by temperature-dependent saturation of $CO_2$ in the thin soil water films. The soil $CO_2$ uptake occurred when the solubility of $CO_2$ was enhanced by the decrease in temperature ($dT/dt < 0$). The symmetric cycle of temperature yielded a diel hysteresis of $F_c$ (Fig. 4d) and the dependency between $F_c$ and $dT/dt$ showed a pinched-hysteresis loop (Fig. 4e).

### 2.4. Effect of the water film $Ca^{2+}$ concentration and pH

Under a modelled diel cycle of temperature (25 ± 10 °C at a dry state of θ ≈ 0.05 $m^3$ $m^{-3}$), we examined the effect of pH variation in the soil water film on $F_c$ (Fig. 5). Here, $Ca^{2+}$ was used to control the chemical status of the film under the assumption of local charge balance. Higher

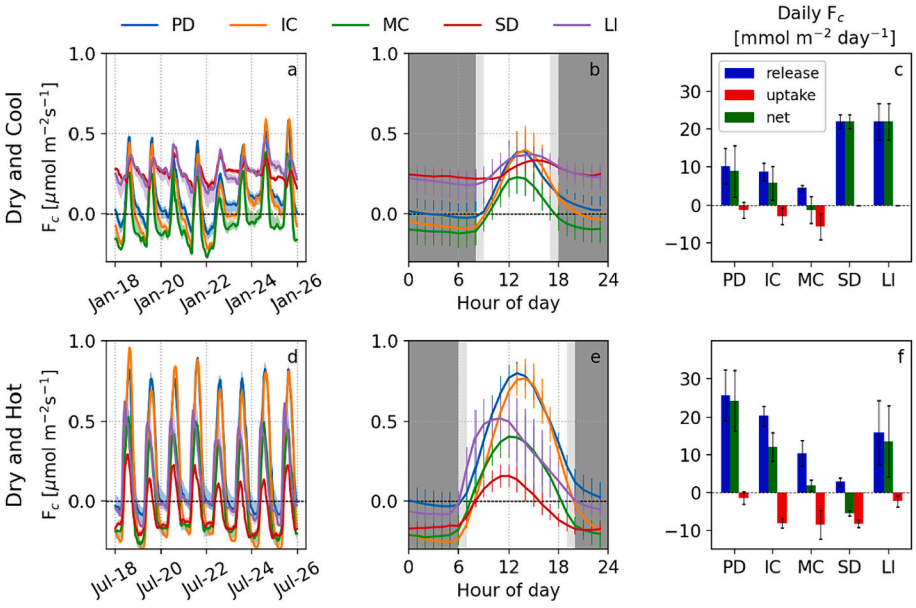


**Fig. 3.** Diel patterns and daily balances of soil-atmosphere $CO_2$ exchange ($F_c$) averaged by crust type during two contrasting dry periods. (a-c) dry and cool (d-f) dry and hot conditions, marked as I and II in Fig. 1. (a and d) Average $F_c$ over a 8-day timespan by crust type: PD, physical depositional crust; (b) IC, incipient cyanobacteria; (c) MC, mature cyanobacteria; (d) SD, lichen community dominated by *Squamarina lentigera* and *Diploschistes diacapsis* and (e) LI, lichen community characterized by *Lepraria isidiata*. Lines are medians and shaded areas delimit the 1st and 3rd quartiles. (b and e) Mean diel cycles with hourly standard deviation over each period. The grey shading indicates nocturnal hours with low photosynthetically active radiation (PAR < 5 µmol m$^{-2}$ s$^{-1}$). (c and f) Daily sum of soil $CO_2$ release, uptake, and resultant net $F_c$ averaged by crust type. Error bars represent one standard deviation.

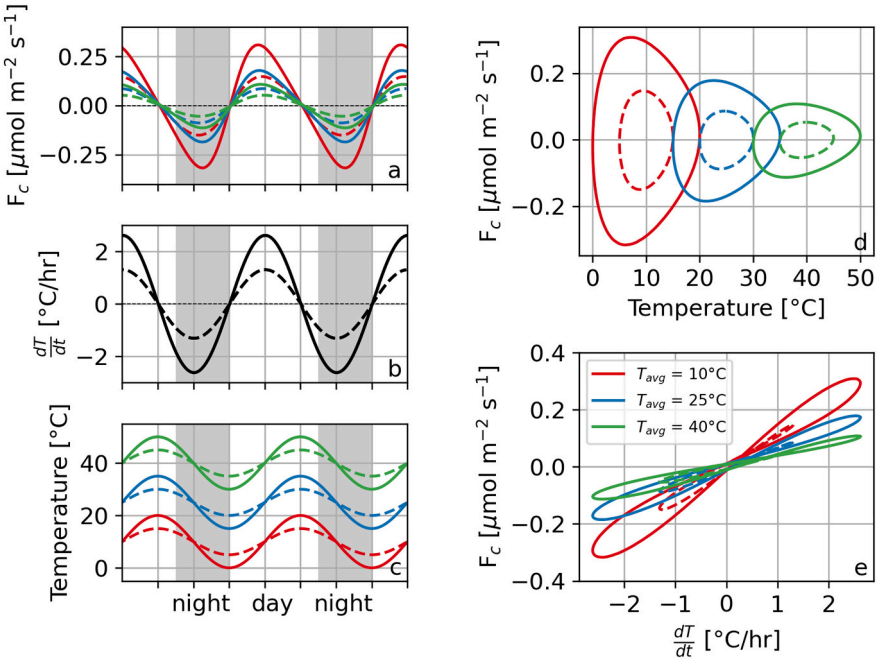


**Fig. 4.** Modelled effect of simulated diel temperature cycle on soil-atmosphere $CO_2$ exchange ($F_c$). (a) Prediction of $F_c$ by the model under a simple temperature cycle, (b) the time derivatives, and (c) the assumed sinusoidal functions (Eq. (1)). We used three mean temperatures ($T_{avg}$): 10 °C (red), 25 °C (blue), and 40 °C (green) with two amplitudes (ΔT): 5 °C (dashed lines) and 10 °C (solid lines). The grey shading indicates fictitious nocturnal hours with decreasing temperature. $F_c$ values are plotted against (d) temperature and (e) time derivatives.

values of $Ca^{2+}$ concentration result in higher pH (lower values of $H^+$ concentration for the charge compensation). The kinetics of inorganic C coupled with diel cycles of temperature had an impact on $F_c$ and local pH in several ways: (1) a more basic pH increased the magnitude of the $F_c$ diel cycle (Fig. 5a); (2) the $CO_2$ solubility dynamics caused the diel cycle of pH with alkalisation during night time (Fig. 5b); (3) depending on chemical conditions, the shape of the hysteresis between $F_c$ and temperature changed (Fig. 5d); (4) higher pH also increased the asynchrony from the temperature-driven solubilisation dynamics shown in Fig. 4. This is summarized in Fig. 5e where the daily $F_c$ minimum ($F_c^{min}$ i.e., the maximum $CO_2$ uptake) and its lag compared to the model driven by temperature alone ($t_{lag}$) are plotted against pH. When the film pH was close to 8 or lower, $F_c$ dynamics could be explained solely by Henry's law (i.e., black dashed lines in Fig. 5a). As the local pH value increased up to

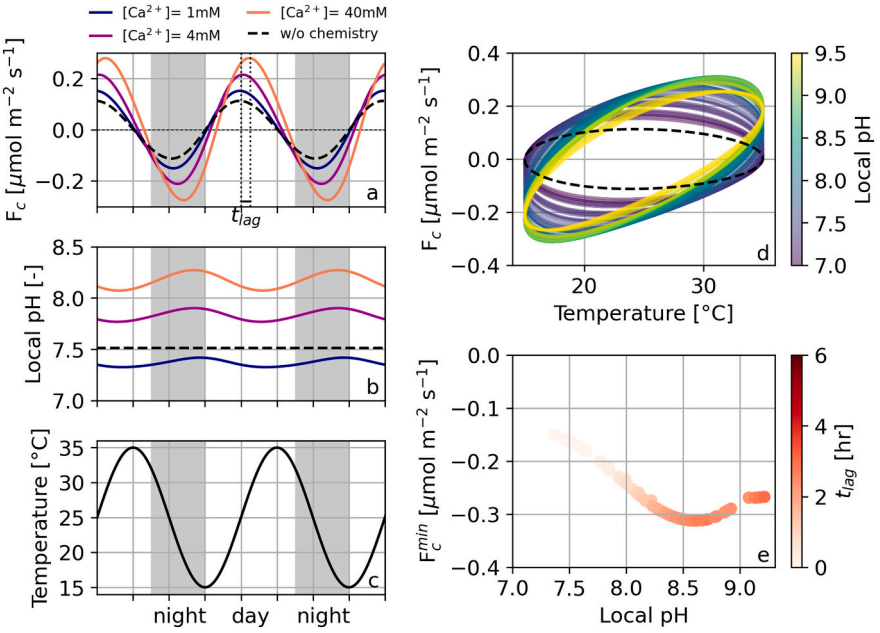


**Fig. 5.** Modelled effect of calcium concentration and pH on soil-atmosphere $CO_2$ exchange ($F_c$) during diel temperature cycles. Different $Ca^{2+}$ concentrations were simulated to modulate pH levels at chemical equilibria. Model predictions of (a) the diel dynamics of $F_c$ and (b) local pH dynamics when (c) a temperature forcing (25 ± 10 °C) is prescribed. The grey shading indicates fictitious nocturnal hours with decreasing temperature. (d) Diel hysteresis between $F_c$ and temperature for varying conditions of local pH. The dashed lines in (a), (b), and (d) correspond to the model prediction without kinetics of DIC species (i.e. when only Henry's law is applied). (e) The $F_c$ minimum ($F_c^{min}$) and its lag compared to the model driven only by Henry's law ($t_{lag}$) as a function of local pH.

pH ~ 8.5, both the magnitude of $F_c^{min}$ and $t_{lag}$ increased, indicating that $CO_2$ dissolution was limited with increased pH. The $CO_2$ uptake reached a maximum at pH 8.5, which corresponds to a transition point between DIC species (i.e., when $HCO_3^-$ starts to decrease and $CO_3^{2-}$ starts to increase). At pH > 8.5, the magnitude of $F_c^{min}$ decreased slightly and stabilized around pH > 9.

### 2.5. Effect of $CO_2$ consumption and productio006E

Effects of additional undifferentiated (i.e., biotic or abiotic) $CO_2$ production and consumption processes other than mineral dissolution in the soil water film were explored by modulating the reaction term $R_{CO_2}(t)$ in (Eq. (3)). Resulting $F_c$ and film pH are displayed in Fig. 6a and b under the prescribed diel temperature cycle (Fig. 6c). The addition of $CO_2$ consumption and production at a constant rate changed the magnitude of $F_c$, inducing a switch from positive to negative values and vice versa (almost constant shifts), and modified $t_{lag}$ in a non-linear manner. The $CO_2$ consumption in the soil water film increased the pH, thus, triggering uptake of atmospheric $CO_2$ for the mass balance at the gas-liquid interfacial surface (green lines in Fig. 6a, b). On the other hand, $CO_2$ production in the soil water film decreased the pH and resulted in $CO_2$ release from the soil (purple lines in Fig. 6a, b). The diel cycle of local pH showed repositioning of the daily maximum and minimum depending on $CO_2$ reaction rates caused by shifts in chemical status (Fig. 6b).

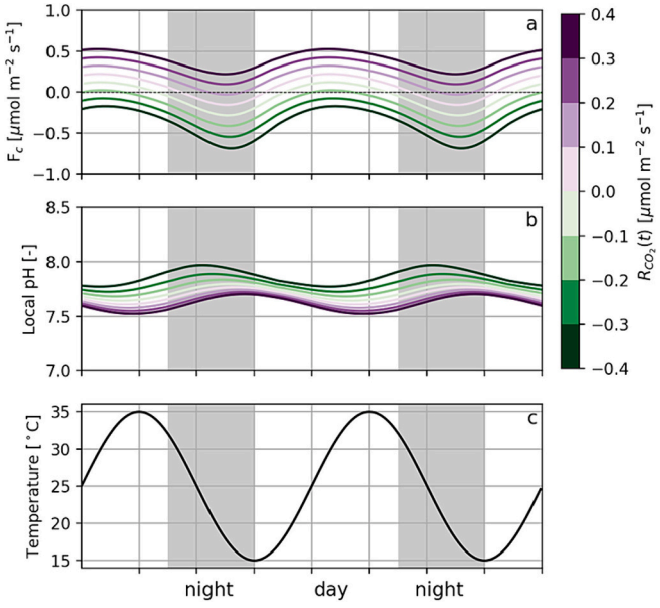


**Fig. 6.** Effect of $CO_2$ consumption and production rate ($R_{CO_2}(t)$) on the soil-atmosphere $CO_2$ exchange ($F_c$). (a) $F_c$ and (b) local pH dynamics of the water film under (c) the sinusoidal temperature cycle (25 ± 10 °C) prescribed. The grey shading indicates fictitious nocturnal hours with decreasing temperature. The purple-green colour scale indicates a constant rate of $CO_2$ consumption (negative $R_{CO_2}(t)$) or $CO_2$ production (positive $R_{CO_2}(t)$) in soil water.

### 2.6. Model prediction of $F_c$ dynamics in physical depositional crusts

By using environmental measurements (Fig. 1b-d), the sfDBM predicted $F_c$ under field conditions. As an example, predicted $F_c$ of physical depositional crusts (where biological activity is assumed to be the lowest) during the selected dry and cool period (marked as period I in Fig. 1) are presented together with field observations (Fig. 7a). Here we present two predictions; (1) the model without chemistry (i.e., in which only Henry's law is considered) and (2) the model including chemical kinetics of DIC species, which captured the $F_c$ diel dynamics more accurately. The patterns and amplitudes of the $CO_2$ uptake and release were well-captured by the latter model without the necessity to incorporate additional processes of $CO_2$ consumption or production. The model also predicted the diel dynamics of soil water pH on soil surface and at 5 cm depth based on the temperature input (Fig. 7b). Alkalization of the medium during nocturnal hours was observed in synchrony with negative $F_c$.

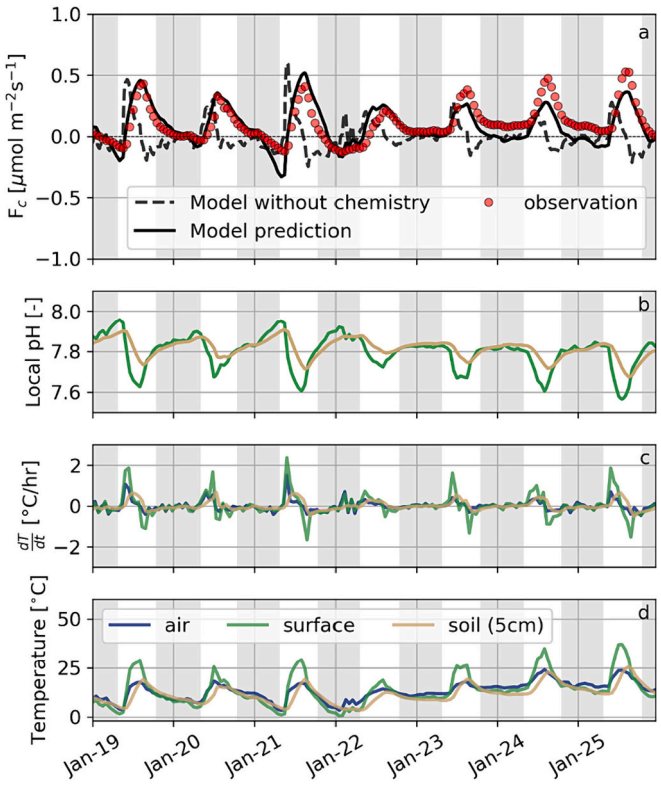


**Fig. 7.** Model prediction of the soil-atmosphere $CO_2$ exchange ($F_c$) for a physical depositional crust during a dry/cool period (period I in Fig. 1). (a) Field observations of $F_c$ (red circles) are compared with predictions by the model without chemistry (dashed black line) and the model including chemistry (solid black line). The grey shading indicates nocturnal hours with low photosynthetically active radiation (PAR < 5 μmol $m^{-2}$ $s^{-1}$). (b) Model prediction of the local pH of the soil water film of surface (green), and soil (brown). (c) Measured temporal derivative of temperature of air (blue), surface (green), and soil (brown). (d) Temperature measurements of air (blue), surface (green), and soil (brown), used as input variables in the model.

### 2.7. Model prediction of abiotically driven $F_c$ along biocrusts succession

By assuming that biological activities are limited during dry periods, we made predictions of abiotically driven $F_c$ during dry/cool – winter and dry/hot – summer periods for different biocrusts along succession ($R_{CO_2}(t) = 0$). Results are shown in comparison with the measured $F_c$ for each crust type (Fig. 8). Overall, the model predictions of abiotically driven $F_c$ are similar to $F_c$ measurements. The timing of maximum $CO_2$ release/uptake matches the model predictions, especially for early stage biocrusts during the dry and cool periods. However, the model underestimated daytime $CO_2$ release during the dry and hot period in early successional stages (PD and IC) and showed the biggest discrepancy under dry and cool conditions for the SD lichen crusts, when $CO_2$ uptake was predicted but not observed.

### 2.8. Potential respiration by biocrusts under dry and cool conditions

According to the model prediction of abiotically driven $F_c$ from different biocrusts, we detected a large deviation from the field observations for the SD crusts under dry and cool conditions (Fig. 8). In Fig. 9, we show the effect of possible additional $CO_2$ consumption and production by SD crusts on the resulting $F_c$ dynamics. Using the model outcome with varying $R_{CO_2}$ values (Fig. 9a), we further estimated the rates of additional $CO_2$ reaction by minimizing the error between the observations and predictions (Fig. 9b) under the given temperature and relative humidity (Fig. 9c). The estimated respiration rates were high when the conditions of PSC ($T_s \leq T_{dew\ point}$) met. By assuming that estimated $R_{CO_2}(t)$ mainly represented the biological activities, we plotted the diel patterns of decomposed biotic (estimated $R_{CO_2}(t)$) and abiotic (observed $F_c(t) - R_{CO_2}(t)$) contributions on $F_c$ compared to the model prediction of abiotically driven $F_c$ when $R_{CO_2} = 0$ (Fig. 9d). The diel patterns show that biological $CO_2$ production offset the abiotic $CO_2$ uptake as it mainly occurred during nighttime. The model prediction of abiotic processes well-aligns with the estimated values, although the modelled uptake rate was slightly lower than the estimated rate during nighttime owing to the chemical effects. In addition, estimated $R_{CO_2}(t)$, the potential respiration, is plotted as a function of $T_s$ and $RH_s$ (Fig. 9e) indicating that respiration was enhanced by the combination of high $RH_s$ and low $T_s$ conditions that were favourable to PSC during this dry period.

## 3. Discussion

For dryland soils covered with biocrusts, one expects daytime $CO_2$ uptake and nighttime $CO_2$ emission to occur due to biocrust photosynthesis and respiration as long as the biocrusts are moist (Tamm et al., 2018; Weber et al., 2018). However, using continuous measurements of the soil-atmosphere $CO_2$ flux ($F_c$) along an ecological succession of biocrusts in calcareous soils, we found that biocrusts at early stages (cyanobacteria) exhibited a substantial nocturnal $CO_2$ uptake under dry conditions (Fig. 2, Fig. 3, Fig. S2, Fig. S3). Only two crust types showed a net daily $CO_2$ uptake during contrasting periods: mature cyanobacterial crusts (MC) showed a net uptake under dry and cool conditions, whereas lichen crusts dominated by *Squamarina lentigera* and *Diploschistes diacapsis* (SD) showed it under dry and hot conditions (Fig. 3 c and f).

Although many dryland soils have been reported to nocturnally absorb $CO_2$ (Sagi et al., 2021), to our knowledge only one study from our site has reported annual estimates of $CO_2$ uptake based on in situ continuous measurements at the soil level (Lopez-Canfin et al., 2022b, 2024). This data is particularly valuable, since reports of larger annual rates obtained by the eddy-covariance measurements have received sharp criticism which questioned the role of abiotic $CO_2$ uptake in the global C cycle (Schlesinger, 2017; Schlesinger et al., 2009). According to the two-year dataset used in our previous study, annual $CO_2$ uptake was $-17 \pm 15$ g C $m^{-2}$ $y^{-1}$ (mean ± spatial standard deviation associated to biocrust succession stages) with a maximum uptake of 55 g C $m^{-2}$ $y^{-1}$. Interestingly, our mean estimate is very close to the uptake flux of 16 g C $m^{-2}$ $y^{-1}$ reported for silicate weathering in a temperate forest (Andrews and Schlesinger, 2001) and close to the upper estimate of calcite precipitation (12.4 g C $m^{-2}$ $yr^{-1}$) reported for drylands (Lal, 2001). Upscaling our average and maximum values to the total surface of drylands (i.e. 66.7 × $10^6$ $km^2$) results in an estimated average and maximum C uptake of ~1.1 and 3.7 Pg $y^{-1}$, respectively, by dryland soils. The magnitude of these values is comparable with the most recent estimate of the missing/residual terrestrial C sink (3.1 ± 0.9 Pg $y^{-1}$) (Houghton et al., 2018). Therefore, even after considering that dryland surfaces absorb C at heterogeneous rates and that biocrust coverages are uncertain, it remains reasonable to assume that the nocturnal $CO_2$ uptake by dryland soils can significantly contribute to balance the global C budget. The potentially overlooked role of non-rainfall water inputs to sustain abiotic $CO_2$ consumption processes in drylands will be discussed later.

Using a mechanistic model with a heuristic approach (i.e., simplified boundary conditions), we highlighted the pivotal role of temperature cycles in determining the magnitude and temporal patterns of $CO_2$ release/uptake under dry conditions (Fig. 4). Due to the temperature-dependency of $CO_2$ solubility (Henry's law) in the water film on soil particles, atmospheric $CO_2$ uptake was predicted when $dT_{soil}/dt < 0$ subject to temporal increase in $CO_2$ solubility. Several studies have already pointed out $dT_{soil}/dt$ as an important driver of the $CO_2$ uptake based on statistical approaches (Sagi et al., 2021). The model in this

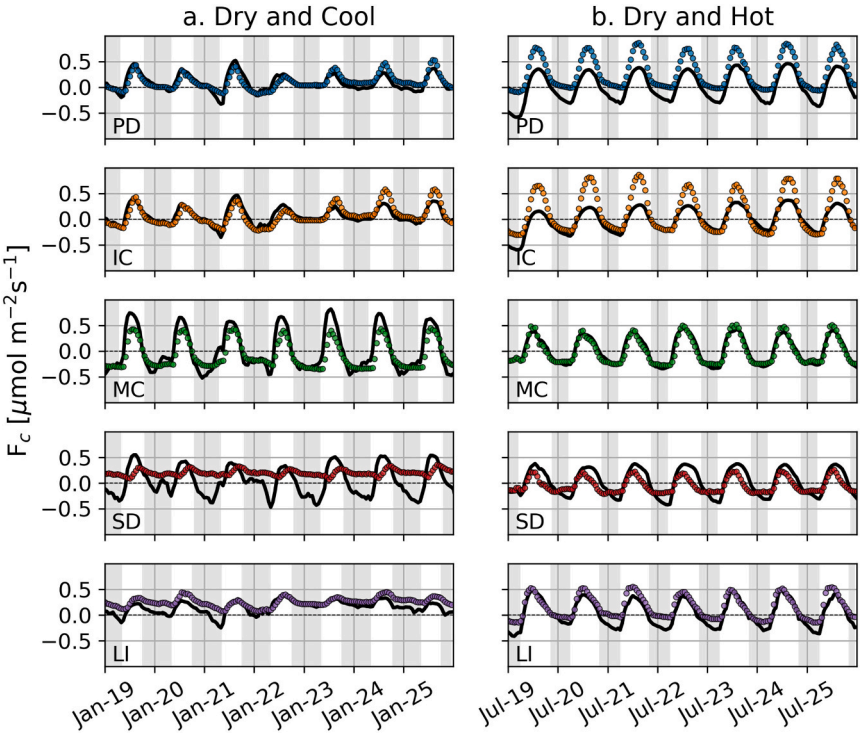


**Fig. 8.** Model predictions of abiotically driven soil-atmosphere $CO_2$ exchange ($F_c$) of different biocrusts during two dry periods with contrasting temperature. Black solid lines indicate the model predictions when $R_{CO_2} = 0$ and circles indicate measurements. The grey shading indicates nocturnal hours with low photosynthetically active radiation (PAR $< 5$ µmol m$^{-2}$ s$^{-1}$). (a) $F_c$ under dry and cool conditions (period I in Fig. 1) (b). $F_c$ under dry and hot conditions (period II in Fig. 1). The predictions are compared to field measurements averaged over replicates for each biocrust type. From top to bottom, results are presented along successional stages; PD, physical depositional crust; IC, incipient cyanobacteria; MC, mature cyanobacteria; SD, lichen community dominated by *Squamarina lentigera* and *Diploschistes diacapsis;* and LI, lichen community characterized by *Lepraria isidiata.*

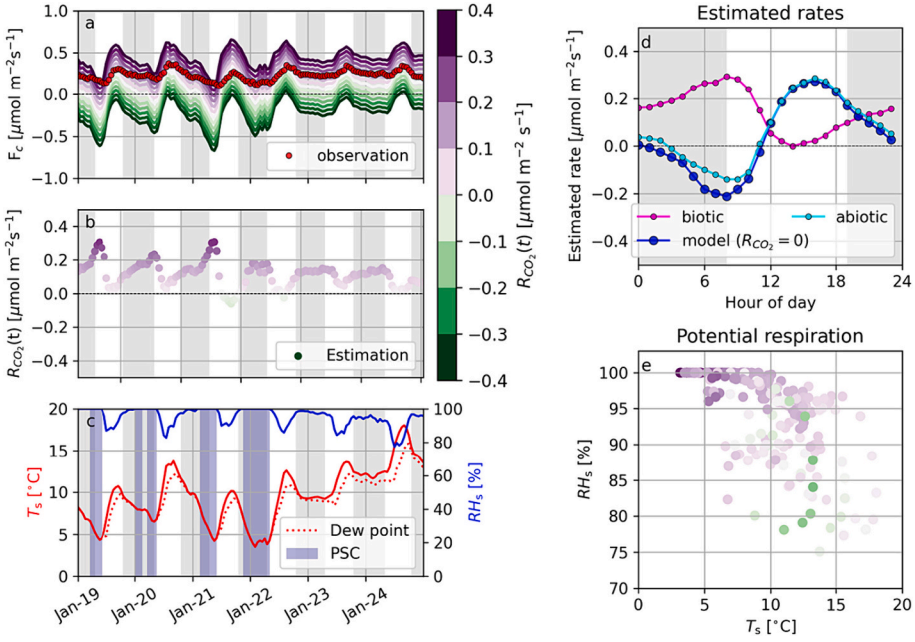


**Fig. 9.** Effects of $CO_2$ consumption and production in a lichen crust community dominated by *Squamarina lentigera* and *Diploschistes diacapsis* (SD) under dry/cool conditions. (a) Model prediction of the soil-atmosphere $CO_2$ exchange ($F_c$) with varying biological contribution $R_{CO_2}(t)$. The purple-green colour scale indicates the constant rate of $CO_2$ consumption (negative $R_{CO_2}(t)$) or $CO_2$ production (positive $R_{CO_2}(t)$) in soil water. (b) Estimated $R_{CO_2}(t)$ values by minimizing the error between the observations and predictions. (c) Diel cycle of soil temperature ($T_s$) and relative humidity in soil ($RH_s$) used as input in the model. The dotted red line indicates the estimated dew point at 5 cm depth and the navy shading indicates the time windows of possible pore-space condensation (PSC). (d) Diel patterns of estimated biotic (magenta) and abiotic (cyan) effects on $CO_2$ dynamics. The blue line indicates the model prediction when $R_{CO_2}(t) = 0$. (e) Estimation of potential respiration by the SD crust as a function of $T_s$ and $RH_s$. The purple-green circles indicate the estimated $R_{CO_2}(t)$ following the same scale as the figure (a) and (b). The grey shading indicates nocturnal hours with low photosynthetically active radiation (PAR $< 5$ µmol m$^{-2}$ s$^{-1}$).

study supports the previous finding with further implications. Here, we show that the diel cycle of temperature ($T_{avg}$ and $\Delta T$) determines the magnitude of $F_c$ exhibiting a diel hysteresis loop, and a pinched hysteresis loop with d$T$/dt (Fig. 4). The hysteresis with $F_c$ lagging after temperature has been explained to be caused by both biological (e.g., transport of photosynthates to the soil) and physical processes (e.g., thermal convection and $CO_2$ diffusion) (Dusza et al., 2020; Fa et al., 2016b; Hamerlynck et al., 2013; Phillips et al., 2011; Riveros-Iregui et al., 2007; Song et al., 2015; Zhang et al., 2015). Here, we showed that under dry conditions the temperature cycle alone can cause a lag of the $CO_2$ uptake and release due to its influence on the $CO_2$ solubility. In addition, the pinched hysteresis between $F_c$ and dT/dt reveals that $CO_2$ dissolution in the soil water film occurs at a slower rate than $CO_2$ degassing in the model.

The magnitude of the $CO_2$ uptake as well as $t_{lag}$ increased under near-basic to high pH values (Fig. 5). At pH > 8.5, most of the dissolved $CO_2$ converts to $HCO_3^-$ or $CO_3^{2-}$ species in the water film, allowing more $CO_2$ to dissolve under Henry's law. Furthermore, the diel cycle of pH in the soil water film was predicted in the model under the assumption of charge balance (Fig. 5b) that are usually not considered in most soil models, where pH values are assumed to be constant (Pumpanen et al., 2003; Šimůnek and Suarez, 1993; Taylor et al., 2017). Our approach of tracking the temporal variation of pH may provide insight into time windows of certain chemical/biological reactions. For instance, alkalization at decreasing temperatures during nighttime (Fig. 5b) may support the formation of $HCO_3^-$ and $CO_3^{2-}$, inducing calcite precipitation and triggering positive feedback for $CO_2$ uptake. This is in agreement with several recent studies which report a rapid translocation of C from atmospheric $CO_2$ to paedogenic carbonates in drylands based on isotopic measurements (Carmi et al., 2019; Liu et al., 2015, 2018, 2020; Wang et al., 2016). However, there is a common conception in the literature according to which $CaCO_3$ dissolution constitutes a $CO_2$ sink while $CaCO_3$ precipitation represents a $CO_2$ source to the atmosphere (Gallagher and Breecker, 2020; Ortiz et al., 2022; Soper et al., 2017) which can seem contradictory to these results. Though this perspective is true in terms of instantaneous gas exchange of the mineral reactions alone, it is less mentioned that $CaCO_3$ dissolution/precipitation are associated with an immediate loss/storage of stable mineral C, respectively. In terms of short-term net C balance, $CaCO_3$ precipitation captures one mole of C from dissolved $CO_2$ that may have an atmospheric origin while $CaCO_3$ dissolution releases on mole of C as dissolved $CO_2$. To correctly assess the net C balance of these reactions over longer periods, transient storage of dissolved $CO_2$ in groundwater, and the presence of other readily available sources of $Ca^{2+}$ need to be considered. Briefly, whether calcite precipitation constitutes a net C sink ultimately depends on the origin of $Ca^{2+}$, with only $Ca^{2+}$ inherited from an external source (other than $CaCO_3$, i.e. Ca-bearing minerals like gypsum and silicates, irrigation water or dust) leading to net C sequestration (Monger et al., 2015; Sanderman, 2012). At our study site where soil contains gypsum, $CO_2$ uptake could be driven by coupled gypsum dissolution- calcite precipitation (Yu et al., 2019), although more empirical evidence is necessary for validation.

When additional $CO_2$ reactions (biotic or abiotic) were considered, the model showed non-linear shifts of $F_c$ dynamics as related to magnitude and temporal asynchrony with temperature (Fig. 6). Overall, $CO_2$ consumption in the soil water film by a third agent, such as dark microbial $CO_2$ fixation (Braun et al., 2021; Spohn et al., 2020) induces alkalization, thus leading to an enhancement of the $CO_2$ uptake. In contrast, $CO_2$ production (e.g., biological respiration) leads to acidification and near-constant shifts in $F_c$ dynamics towards $CO_2$ release (Fig. 6b). Most $F_c$ research has focused on soil $CO_2$ production and assumed soil $CO_2$ consumption processes as being negligible. Under close to neutral/acidic conditions, considering only the effect of abiotic and biotic $CO_2$ production may be reasonable because the effects of DIC fractionation and mineralization are minimized. However, for basic conditions like those of dryland alkaline soils, contributions of abiotic and biotic $CO_2$ reactions to $F_c$ dynamics do not obey a simple additive relation. This is why detailed reaction dynamics in space and time need to be analysed and an adequate upscaling strategy of soil processes with highly heterogeneous water availability, biological activity and mineral distributions needs to be developed.

Investigating $F_c$ dynamics over the ecological succession of biocrusts yielded the unexpected outcome that biological activities and their masking effects on the abiotic $CO_2$ uptake under dry conditions are not linearly related with biocrust successional stages with increasing SOC content (Figs. 7, 8, 9, and Fig. S5). Other factors such as soil pH (or amount of cations) and/or other physical properties affect the magnitude and diel patterns of $F_c$ dynamics under various conditions as shown in the model. We indeed found similar patterns with soil pH, and also the relative fraction of cyanobacteria (Miralles et al., 2020) in the microbial communities (Fig. S5). Under a diel cycle of temperature, the optimum soil pH for $CO_2$ uptake is around 8.5 (Fig. 5e) which is associated with enhanced carbonate precipitation and coincides with the pH of mature cyanobacterial crusts (MC) (Fig. S5) that exhibited the highest nocturnal $CO_2$ uptake over the whole succession (Fig. 3 and Fig. S3). In fact, Cyanobacteria might have enhanced this uptake by inducing this pH alteration. They are known to have a $CO_2$ concentrating mechanism (CCM) that induces alkalization by releasing $OH^-$ into the surrounding medium during photosynthesis (Büdel et al., 2004; Garcia-Pichel and Belnap, 1996). In addition, they have also been suggested to promote gypsum dissolution to extract its water of crystallization (Huang et al., 2020), potentially fostering $CaCO_3$ precipitation through $Ca^{2+}$ release by weathering of gypsum or Ca-silicates (Jansson and Northen, 2010). It is therefore reasonable to expect cyanobacterial contributions to $CaCO_3$ accumulation in biocrust soils enhancing $CO_2$ uptake.

The net $CO_2$ uptake by biocrusts was greatly reduced in lichenized late successional stages (SD and LI) compared to early stages (IC and MC) (Fig. 2). As larger organisms like lichens or mosses develop in late stages of the succession, the abundance of cyanobacteria decreases while SOC increases (Miralles et al., 2020). The activity of green algal lichens is known to lower the pH of surroundings by secreting organic acids, and to increase SOC content (Ghiloufi et al., 2023), hence inhibiting the abiotic processes of $CO_2$ dissolution and precipitation of carbonates. Similarly, the $CO_2$ uptake and release by soil were also lower and higher, respectively, in the physical depositional crusts compared to cyanobacterial crusts (IC and MC) (Fig. 2). While the reduced $CO_2$ uptake can be attributed to the lowest pH under the influence of the lowest calcium carbonate contents, the substantial $CO_2$ release (Fig. 1b) is likely due to greater $T_s$ fluctuations enhancing non-diffusive $CO_2$ transport by thermal convection (Ganot et al., 2014; Phillips et al., 2011; Roland et al., 2013; Spohn and Holzheu, 2021).

Some studies using chamber measurements have also attributed the $CO_2$ uptake by dryland soils to thermal convection and expansion/contraction of soil air (Fa et al., 2016b; Gao et al., 2021; Yang et al., 2020). However, although we acknowledge that such processes can play a significant role in $CO_2$ transport within the soil-atmosphere continuum, here we postulate that they alone cannot explain the observed $CO_2$ uptake as it arose from the $CO_2$ molar fraction ($\chi_c$) of soil dropping below atmospheric $\chi_c$ values. Therefore, this necessarily involves $CO_2$ consumption, not only $CO_2$ transport which would at best equilibrate soil $\chi_c$ with atmosphere $\chi_c$. Although our model does not include thermal convective venting, most of the $F_c$ variation was explained by the temperature- and pH-driven dissolution dynamics of $CO_2$ in the top soil.

This study focuses on the mechanisms of nocturnal $CO_2$ uptake under dry conditions. With limited water availability for biological activity, $F_c$ dynamics could be explained mostly by abiotic processes like in physical depositional crusts (Figs. 7 and 8). This agrees with the previous finding that biocrust respiration is close to zero during summer in response to the extreme drought and thermal stress (Miralles et al., 2018). Therefore, differences in $F_c$ dynamics among crust types during drought were related to edaphic properties and environmental conditions. However, the model revealed that SD crusts during wintertime (dry/cool

conditions) were able to maintain biological respiration under high $RH_s$ through possible pore-space condensation (PSC) (Fig. 9). Although the water content was low during this period ($\theta \sim 0.06\ m^3\ m^{-3}$), biological activity could be temporally enabled by non-rainfall water input such as PSC, since soil air was regularly close to saturation with respect to water vapor ($RH_s \sim 100$ %) with temperature meeting the condition for PSC, in contrast to the dry and hot summer periods when $RH_s$ values were frequently below 50 % and temperature was too high to induce PSC (Fig. 1b and c). This supports the finding that lichens, especially of *D. diacapsis* studied here, can regain metabolic activity even at low water contents in presence of high relative humidity (Baldauf et al., 2021; Richardson, 2002).

In the model, we use the effective water film thickness as the hydrological basis that enables chemical reactions and biological activity even under relatively dry conditions. The effective water film thickness is estimated from measured water contents at daily scale. Furthermore, in this study, we assume the homogeneity of physical structures for simplified upscaling (fixed soil physical parameter, Table S5). However, biocrusts create a discontinuous boundary at the interface between soil and atmosphere, as well as micro-scale heterogeneity in terms of soil porosity, texture, and distribution of biological and chemical substances (Kim and Or, 2017, 2019; Kratz et al., 2022). This structural effect becomes crucial under wet conditions, especially owing to the swelling-shrinking dynamics of extracellular polymeric substances in the biocrusts influencing the properties of liquid-gas transport (Kidron et al., 2020; Sun et al., 2022, 2023). However, under dry conditions near the surface, gas transport may not be limited by structural obstacles, and can even be enhanced due to crust-cracking, which possibly caused the increased $F_c$ during summertime in PD and IC crusts (Fig. 8b). Therefore, we argue that, under dry conditions, our approach using the effective water film thickness was reasonable to estimate $F_c$ and yielded good predictions.

The notion of water film thickness can be further extended by including adsorption and condensation processes under the mass conservation rule of water vapor within soils (Tuller et al., 1999). The adsorption of atmospheric water vapor by soil has been shown to potentially drive the nocturnal $CO_2$ uptake in summer at this site (Lopez-Canfin et al., 2022a). Here, we additionally show that outside of summer periods, whereas surface conditions of temperature and relative humidity at the soil-atmosphere interface are often unfavourable to dew formation (Agam and Berliner, 2006; Lopez-Canfin et al., 2022a), these conditions in the soil below crusts were frequently favourable to PSC at night (Fig. S4). Especially after major rain events, we observe that below-crust soils sustained high $RH_s$ allowing condensation to occur within soil pores and the conditions could last days or even weeks depending on precipitation and crust types (Fig. 1c). This implies that biocrusts may contribute to the prolonged storage of rain and its possible usage to sustain biological activity in drylands even at the small scale, which would mirror the processes at landscape scale (Baldauf et al., 2023; Eldridge et al., 2020). We argue that due to the immense surface area of inner soils (especially in fine-textured soils) compared to the soil surface, the water storage effect through PSC can be substantial in drylands. By contrast, it has been stated that the lack of water in drylands would prevent $CO_2$ uptake associated with the dynamics of Ca-bearing minerals (Schlesinger et al., 2009). However, after considering the contribution of overlooked non-rainfall water inputs (PSC and water vapor adsorption), our annual estimates of $CO_2$ uptake may be compatible with rates of $CO_2$-consuming mineral reactions. Hence, further research is necessary to provide quantitative estimates of water vapor adsorption and PSC and their coupling with many ecosystem functions in drylands (Wang et al., 2017). This is of major importance as climate change is expected to affect the duration and frequency of wet conditions as well to increase the extension of dry conditions in time and space (Grünzweig et al., 2022).

## 4. Conclusions

The objective of this research was to unravel the main mechanism responsible for the nocturnal $CO_2$ uptake by soil and biocrusts in drylands using a mechanistic model. We focused on dry periods, during which biological activity is minimized but a thin water film remains on the surface of soil particles possibly sustained by water vapor adsorption and pore-space condensation. Under these conditions, abiotic processes alone can predict most of the nocturnal $CO_2$ uptake; in particular, dissolution/degassing of $CO_2$ driven by temperature dynamics in combination with diel pH variations in the soil water film. The alkalization of the water film at night, with pH conditions >8.5, is particularly favourable for $CO_2$ uptake and calcite precipitation in agreement with the maximum $CO_2$ uptake measured in mature cyanobacterial crusts. By consuming or producing $CO_2$ and modifying the pH of the soil water film, biocrusts further modulate carbon dynamics. The coupling between water and inorganic C cycling in drylands has been largely understudied compared to mesic ecosystems, and therefore further research is required to better constrain their rates and confirm that the mechanism of $CO_2$ uptake unravelled in this study is widespread. Expecting changes in precipitation, temperature, and disturbance regimes globally, it is becoming increasingly important to comprehend and forecast the soil-atmosphere $CO_2$ exchange capacity of drylands, especially regarding biocrusts as the primary carbon sequester. By elucidating temperature-water-carbon processes within biocrusts, this study provides a missing puzzle piece of nocturnal $CO_2$ uptake and emphasizes the interplay between abiotic processes and soil biological agents mitigating $CO_2$ emissions in the face of changing climates.

## 5. Material and methods

### 5.1. Experimental site

The measurements were conducted in the experimental site of El Cautivo (N 37°00′37″, W 2°26′30″, ~ 250 m a.s.l), an area of badlands located in the Tabernas Desert. The climate is classified as semi-arid thermo-Mediterranean with a mean annual temperature of 18 °C and mean annual precipitation of 230 mm. The soil is classified as a silty-loam with >60 % gypsum-calcareous and siliceous particles of silt-size, 20–30 % fine sand, 5–10 % clay. The calcium carbonate equivalent content ranges from 11 % to 28 % and gypsum content is highly heterogeneous between 0.1 % to 35 %. A detailed pedological characterization of the soil horizons can be found in Cantón et al., 2003 and soil properties specific to the 0–5 cm horizon are detailed in Lopez-Canfin et al., 2022b.

A third of the territory is bare and eroded soil and another third is covered by short vascular vegetation with biocrusts in the interspaces. The rest is covered mainly by biocrusts. Five different biocrust types can be distinguished and assigned to stages of ecological succession (Lázaro et al., 2008): (1) physical depositional crust (PD); (2) incipient cyanobacteria-dominated crust (IC); (3) mature cyanobacteria-dominated crust (MC); (4) lichen-dominated crust with *Squamarina lentigera* (Web.) Poelt and *Diploschistes diacapsis* (Ach.) Lumbsch as key species (SD); and (5) lichen-dominated crust with *Lepraria isidiata* (Llimona) Llimona and Crespo as key species (LI). Lichen-dominated stages (SD and LI) were considered as late successional stages while previous stages were considered as early successional stages (PD, IC and MC) (Fig. S1).

### 5.2. Environmental measurements

Continuous measurements of soil and above-surface variables were conducted from February 2018 to December 2019. At 5 cm depth, the $CO_2$ molar fraction ($\chi_c$) was measured by GMP252 and GMM222 probes (total of 14 and 3 probes, respectively) (Vaisala, Vantaa, Finland; hereafter Vaisala). All GMP252 sensors were new and GMM222 sensors

were calibrated for $CO_2$ just before installation by using the GMK220 carbon dioxide calibrator (Vaisala) and a two-points calibration curve: using (variable but known) ≈ 350 ppm and ≈ 1500 ppm for spans. The soil water content (θ) was measured at 5 cm depth, below crusts, by EC-5 and 5TM sensors (Meter Group, Pullman, WA). The θ sensors were calibrated using the manufacturer's general equation for mineral soils. All mineral soils up to an electrical conductivity (EC) of 8 dS $m^{-1}$ in saturation extract should be covered by this equation, according to the manufacturer's instructions. In 1:5 soil-to-water ratios, preliminary testing revealed that most soils at our study site had an EC < 1 dS $m^{-1}$. Based on those values, it was reasonable to expect that EC in saturation extracts would not exceed the recommended threshold (Kargas et al., 2020). The 5TM sensors measured the soil temperature ($T_s$) that was also measured with thermistors (108, Campbell Scientific, Logan, UT, USA; hereafter CSI). All these measurements were performed in the different biocrust types in triplicates. Since mature cyanobacterial patches were also present within the SD site, for comparison purpose, measurements were also performed for this MC crusts within the SD site in duplicate, thus results in five MC replicates. Within each biocrust type, the relative humidity at 5 cm depth and in the atmosphere directly in contact with soil ($RH_s$ and $RH_a$, respectively) were measured with iButton® DS1923 loggers (Maxim Integrated, San Jose, CA, USA); air temperature ($T_a$) and relative humidity at 30 cm aboveground were measured by a S-THB-M006 Smart Sensor (Onset Computer Corporation, Bourne, MA, USA; hereafter Onset); surface temperature ($T_{surf}$) was measured by a S-TMB-M0xx Smart Sensor (Onset) and the photosynthetically active radiation (PAR) by a S-LIA-M003 Smart Sensor (Onset); precipitation was measured by a Rain-O-Matic-Pro tipping-bucket rain gauge of 0.25 mm resolution (Pronamic, Ringkoebing, Denmark) at 1.5 m above the ground surface. At 2 cm aboveground, atmosphere $\chi_c$ was monitored in the PD and SD sites by GMP252 probes (Vaisala), and atmospheric temperature and pressure was monitored in the LI site by a SP1A air pressure transmitter (PM Ecology, Gdynia, Poland). The rain gauge was connected to an on–off Hobo Event data logger (Onset) and all other variables were measured every 30 s and stored as 20-min averages by data-loggers CR1000 (CSI) and H21 (Onset). More details about this experimental design can be found in Lopez-Canfin et al., 2022a.

### 5.3. $CO_2$ flux calculation and gap-filling

Measurements in different time resolutions were harmonized to hourly averages. Then, the whole dataset was split into subsets of variables of the same type (e.g. temperatures) and each subset was imputed separately to avoid generating spurious correlations. A non-parametric method based on random forests was chosen to calculate missing values (Stekhoven and Bühlmann, 2012), as the method can deal with mixed-type data and is particularly effective in handling complex interactions and non-linear data structures.

The soil-atmosphere $CO_2$ fluxes ($F_c$) were estimated from $\chi_c$ using the gradient method based on Fick's first law of molecular diffusion: $F_c = -\rho_a k_s \frac{d\chi}{dz}$ where $F_c$ is the soil-atmosphere flux ($\mu$mol $m^{-2}$ $s^{-1}$), $\rho_a$ is the average molar density of air (mol $m^{-3}$), $d\chi$ is the difference in $CO_2$ molar fraction ($\mu$mol $mol^{-1}$) between atmosphere and soil, and $dz$ is the vertical difference between atmosphere and soil (m), $k_s$ is the $CO_2$ diffusion coefficient or empirical soil transfer coefficient ($m^2$ $s^{-1}$), calibrated empirically from flux chamber measurements as previously recommended (Sánchez-Cañete et al., 2017)). Negative $F_c$ values correspond to $CO_2$ uptake from the atmosphere to the soil (i.e., influx) whereas positive fluxes correspond to $CO_2$ release from the soil to the atmosphere (i.e., efflux). Further details about the flux estimation are available in Lopez-Canfin et al. (2022b, 2024).

### 5.4. Classification of wet/dry and cold/hot periods

We split the dataset in wet/dry and cool/hot periods for subsequent data analysis. Based on daily averaged values of θ and $T_a$ during the whole measurement period (from February 2018 to December 2019), each day was classified as wet or dry and cold or hot. To perform these classifications, θ and $T_a$ thresholds were selected based on the principle of minimizing cross-entropy. For the automated threshold selection, we used an algorithm that does not make any a priori assumption on the underlying distribution of values (Li and Lee, 1993). The daily classification was performed for each site to consider the effect of microclimate on biotic and abiotic processes. The result of the classification process defines four distinctive periods: (a) dry and cool, (b) wet and cool, (c) dry and hot, and (d) wet and hot. Based on this output, we selected two dry sub-periods with contrasting temperature to compare the field observations and the model predictions of the $F_c$ time series; (I) dry and cool (from 2019-01-18 to 2019-01-25, θ = 0.05 ± 0.03 $m^3$ $m^{-3}$; $T_s$ = 11.08 ± 3.97 °C; $RH_s$ = 95.61 ± 5.82 %); (II) dry and hot (from 2019-07-18 to 2019-07-25, θ = 0.04 ± 0.02 $m^3$ $m^{-3}$; $T_s$ = 33.50 + 6.92 °C; $RH_s$ = 49.36 ± 7.93 %). These two periods are marked as grey shaded area in Fig. 1.

### 5.5. Mechanistic modelling of $CO_2$ fluxes from biocrusts

The influence of abiotic and biotic processes on $F_c$ was explored mechanistically by using the desert biocrust model (DBM) (Kim and Or, 2017, 2019). The DBM simulates biophysical and chemical processes in biocrusts (including biotic and abiotic C and N-cycling) under dynamic conditions of hydration, light, and temperature. In this study, the individual-based description of microbial activity was replaced by a population-based description to elucidate the chemical processes that are influenced by biological processes. Furthermore, we included a module of gypsum dissolution and calcite precipitation dynamics.

In this study, we investigated the roles of temperature dynamics on $F_c$ under field conditions. Unlike the previous release of the model that simulated pre-assigned laboratory conditions of temperature and water dynamics (Kim and Or, 2017, 2019), we used environmental measurements as input variables for boundary conditions; soil water content (θ), air-surface-soil temperature ($T_a$, $T_{surf}$, $T_s$) for the temperature profile, and atmospheric $CO_2$ molar fraction ($\chi_c$). The porosity and soil pH values were also used to set initial conditions of the physical/chemical soil domain at the interface with atmospheric conditions. The detailed model description is provided in the supplementary information. The modified DBM in this study is named as the simplified field DBM (sfDBM) and the script written in Python 3 is archived on Zenodo (Kim, 2024).

Although a realistic empirical input is required to ultimately test the model prediction of $F_c$, the interactive effect of many variables complexifies interpretation under field conditions. Therefore, in order to understand the mechanisms and to disentangle tightly coupled processes involved in the $CO_2$ uptake, we first used a heuristic approach, which is a simplified learning method to test the effect of a reduced set of variables controlled by model simulations. Following this approach, simplified boundary conditions of temperature were used to evaluate the effect of temperature. To this end, a diel temperature cycle was simulated with a periodic function at a fixed hydration condition (a dry condition equivalent to θ ~ 0.05 $m^3$ $m^{-3}$, which is about 0.03 g $g^{-1}$). Here, we used a sinusoidal function to simulate a diel cycle of air temperature as follows:

$$T(t) = T_{avg} + \Delta T sin\left[\frac{2\pi}{24}(t-6)\right], \quad (1)$$

where $T_{avg}$ is the mean and $\Delta T$ is the amplitude of a diel temperature cycle [°C], t is the time in the unit of hour [hr]. With this function, the temperature minimum $T_{avg} - \Delta T$ occurs at $t = 0$ and the maximum $T_{avg} + \Delta T$ at $t = 12$ [hr] (Fig. 4c). Regarding the chemical effect of inorganic C partitioning, the $Ca^{2+}$ content in the water film was used as a representative control parameter of pH. Other input

parameters used in this work are listed in the supplementary information.

The essential process in this model is the solubility of $CO_2$ which is a function of the temperature dependent solubility (Sander, 2015);

$$H_{cc}(T(t)) = H_{cc}^{\Theta} e^{-\frac{\Delta_{soln}H}{R}\left(\frac{1}{T(t)+273.15}-\frac{1}{T^{\Theta}}\right)}, \quad (2)$$

where $H_{cc}^{\Theta} \equiv k_H R T^{\Theta}$ is the gas-specific (here, e.g., $CO_2$) dimensionless Henry's constant. The superscript $\Theta$ refers to the standard temperature condition at $T^{\Theta} = 298.15K$, $\Delta_{soln}H$ is the enthalpy, and $R$ is the gas constant. According to this Arrhenius formular, the solubility increases with decreasing temperature.

$$C^{l,*}(\vec{r},t) = H_{cc}(T(t))C^{g}(\vec{r},t), \quad (3)$$

where $C^{l,*}(\vec{r},t)$ is the concentration of dissolved $CO_2$ in soil water at equilibrium and $C^{g}(\vec{r},t)$ is the concentration of gaseous $CO_2$ at a position $\vec{r}$ at time $t$ based on the temperature dependent air-density $\rho^{g}(T(t))$ and the partial pressure of $CO_2$, $p_{CO_2}(t)$, resulting $C^{g}(\vec{r},t) = \rho^{g}(T(\vec{r},t))p_{CO_2}(t)$. Here, the temperature-dependent air density includes the effect of thermal expansion and contraction. We use observed partial pressure of $CO_2$ in the air and in soil at 5 cm depth as model inputs and the thermal convection from deeper soils are not considered in this work. The concentration of dissolved $CO_2$, $C^{l}(\vec{r},t)$, can be calculated based on the diffusion-convection-reaction equation with the mass transfer term based on the Henry's law:

$$\frac{\partial C^{l}(\vec{r},t)}{\partial t} = \frac{dC^{l}(\vec{r},t)_{degassing}}{dt} + \frac{dC^{l}(\vec{r},t)_{diffusion}}{dt} + \frac{dC^{l}(\vec{r},t)_{convection}}{dt} + \frac{dC^{l}(\vec{r},t)_{reaction}}{dt}$$

$$= -k_L a\left(C^{l}(\vec{r},t) - C^{l,*}(\vec{r},t)\right) + \nabla\cdot\left(D(\vec{r},t)\nabla C^{l}(\vec{r},t)\right) - \nabla\cdot\left(\vec{v}C^{l}(\vec{r},t)\right) + R(t)$$

$$\approx -k_L a\left(C^{l}(\vec{r},t) - H_{cc}(T(t))C^{g}(\vec{r},t)\right) + R_{chem}(t) + R_{CO_2}(t), \quad (4)$$

where $k_L$ is the mass-transfer coefficient and $a$ is the gas-liquid interfacial surface area and $D(\vec{r},t)$ is a diffusion coefficient which is a function of position and time. However, we assume that on the top soil $k_L a \gg D(\vec{r},t)$ and the convection on the liquid phase is negligible under dry conditions, thus Eq. (4) is used for calculating $C^{l}(\vec{r},t)$. Here, the reaction terms are described with two factors; $R(t) \approx R_{chem}(t) + R_{CO_2}(t)$ where $R_{chem}(t)$ indicates the chemical reactions under the explicit kinetics with the charge conservation constraint and $R_{CO_2}(t)$ is an additional source/sink of $CO_2$. Since the major chemical contributions are already included in $R_{chem}(t)$, $R_{CO_2}(t)$ can be interpreted as biological contributions such as respiration (positive) or fixation (negative). $R_{CO_2}(t)$ can vary in time, however, in our heuristic approach, we assumed the reaction rates are constant to investigate the roles of additional production or consumption of $CO_2$.

By assuming that the gas-liquid partitioning of gases under Henry's law, concentration of $CO_2$, in liquid and gas phases, $C^{l}(\vec{r},t)$ and $C^{g}(\vec{r},t)$ respectively, can be calculated at each time step. Between the interval $\Delta t$, the amount of degassed $CO_2$ (loss from the liquid phase calculated based on Eqs. (3) and (4) under the principle of mass conservation) is defined as the gaseous efflux of $CO_2$, $F_c(\vec{r},t)$, which is calculated as follows:

$$F_c(\vec{r},t) = \frac{1}{\Delta t}\int_t^{t+\Delta t} \frac{dC^{g}(\vec{r},\tau)_{degassing}}{d\tau} + \frac{dC^{g}(\vec{r},\tau)_{diffusion}}{d\tau} + \frac{dC^{g}(\vec{r},\tau)_{convection}}{d\tau} d\tau$$

$$\approx \frac{1}{\Delta t}\int_t^{t+\Delta t} \frac{dC^{g}(\vec{r}\tau)_{degassing}}{d\tau} d\tau$$

$$F_c(t) = \iint k_L a\left(C^{l}(\vec{r},t) - H_{cc}(T(t))\rho^{g}(T(\vec{r},t))p_{CO_2}(t)\right)dt d\vec{r} \quad (5)$$

In this work, in the calculation of the gaseous concentration of $CO_2$, convective flow and diffusion is ignored by assuming the dominant process as the degassing by temperature-dependent solubility dynamics. However, by including the temperature dependent air density, thermal expansion and related dilution effect is included indirectly in the model. Details of kinetics included in the model are described in the previous publications and supplementary information (Kim and Or, 2017, 2019). The script of sfDBM in Python 3 is available in Github (https://github.com/Graz-Institute-of-Biology/sfDBM_STOTEN) and archived on Zenodo (Kim, 2024). Used parameters and input variables for the soil models are provided in the supplementary information and supplementary data.

## CRediT authorship contribution statement

**Minsu Kim:** Writing – review & editing, Writing – original draft, Visualization, Validation, Software, Methodology, Formal analysis, Conceptualization. **Clément Lopez-Canfin:** Writing – review & editing, Writing – original draft, Validation, Methodology, Investigation, Data curation, Conceptualization. **Roberto Lázaro:** Writing – review & editing, Resources, Investigation, Funding acquisition. **Enrique P. Sánchez-Cañete:** Writing – review & editing, Resources, Investigation, Funding acquisition. **Bettina Weber:** Writing – review & editing, Supervision, Conceptualization.

## Declaration of competing interest

The authors declare that they have no known competing financial interests or personal relationships that could have appeared to influence the work reported in this paper.

## Data availability

The model scripts is available in a GitHub repository (https://github.com/Graz-Institute-of-Biology/sfDBM_STOTEN) and archived on Zenodo (https://doi.org/10.5281/zenodo.10843357)

## Acknowledgements

M.K. discloses support for the research of this work from Swiss National Science Foundation [grant number P400P2_191119]. This work was also supported by the Spanish Ministry of Economy and Competitiveness through projects DINCOS (CGL2016-78075-P) and INTEGRATYON$^3$ (PID2020-117825GB-C21 & C22), and by ICAERSA (P18-RT-3629) and MORADO (C-EXP-366-UGR23) of the Andalusian Regional Government including European Union ERDF funds. C.L.C acknowledges the "Margarita Salas" grant founded by the European Union – NextGenerationEU and the Spanish Ministry of Universities through the University of Granada, and the OASIS project funded by European Union's Horizon research and innovation programme under the Marie

Skłodowska-Curie grant agreement No 101109110. Views and opinions expressed are however those of the author(s) only and do not necessarily reflect those of the European Union (EU) or the European Research Executive Agency (REA). Neither the EU nor the REA can be held responsible for them. The authors acknowledge the financial support by the University of Graz.

## Appendix A. Supplementary data

Supplementary data to this article can be found online at https://doi.org/10.1016/j.scitotenv.2024.171751.

## References


Agam, N., Berliner, P.R., 2006. Dew formation and water vapor adsorption in semi-arid environments—a review. J. Arid Environ. 65, 572–590. https://doi.org/10.1016/j.jaridenv.2005.09.004.

Andrews, J.A., Schlesinger, W.H., 2001. Soil CO2 dynamics, acidification, and chemical weathering in a temperate forest with experimental CO2 enrichment. Global Biogeochem. Cycles 15, 149–162. https://doi.org/10.1029/2000GB001278.

Baldauf, S., Porada, P., Raggio, J., Maestre, F.T., Tietjen, B., 2021. Relative humidity predominantly determines long-term biocrust-forming lichen cover in drylands under climate change. J. Ecol. 109, 1370–1385. https://doi.org/10.1111/1365-2745.13563.

Baldauf, S., Cantón, Y., Tietjen, B., 2023. Biocrusts intensify water redistribution and improve water availability to dryland vegetation: insights from a spatially-explicit ecohydrological model. Front. Microbiol. 14, 1179291. https://doi.org/10.3389/fmicb.2023.1179291.

Benzerara, K., Skouri-Panet, F., Li, J., Férard, C., Gugger, M., Laurent, T., Couradeau, E., Ragon, M., Cosmidis, J., Menguy, N., Margaret-Oliver, I., Tavera, R., López-García, P., Moreira, D., 2014. Intracellular Ca-carbonate biomineralization is widespread in cyanobacteria. Proc. Natl. Acad. Sci. 111, 10933–10938. https://doi.org/10.1073/pnas.1403510111.

Braun, A., Spona-Friedl, M., Avramov, M., Elsner, M., Baltar, F., Reinthaler, T., Herndl, G.J., Griebler, C., 2021. Reviews and syntheses: heterotrophic fixation of inorganic carbon – significant but invisible flux in environmental carbon cycling. Biogeosciences 18, 3689–3700. https://doi.org/10.5194/bg-18-3689-2021.

Büdel, B., Weber, B., Kühl, M., Pfanz, H., Sültemeyer, D., Wessels, D., 2004. Reshaping of sandstone surfaces by cryptoendolithic cyanobacteria: bioalkalization causes chemical weathering in arid landscapes. Geobiology 2, 261–268. https://doi.org/10.1111/j.1472-4677.2004.00040.x.

Cantón, Y., Solé-Benet, A., Lázaro, R., 2003. Soil–geomorphology relations in gypsiferous materials of the Tabernas desert (almeria, SE Spain). Geoderma 115, 193–222. https://doi.org/10.1016/S0016-7061(03)00012-0.

Carmi, I., Kronfeld, J., Moinester, M., 2019. Sequestration of atmospheric carbon dioxide as inorganic carbon in the unsaturated zone under semi-arid forests. CATENA 173, 93–98. https://doi.org/10.1016/J.CATENA.2018.09.042.

Chamizo, S., Cantón, Y., Rodríguez-Caballero, E., Domingo, F., 2016. Biocrusts positively affect the soil water balance in semiarid ecosystems. Ecohydrology 9, 1208–1221. https://doi.org/10.1002/eco.1719.

Chen, Y., Lian, B., Yin, Z., Tang, Y., 2014. Weathering of carbonate rocks by biological soil crusts in karst areas. J. Earth Sci. 25, 662–667. https://doi.org/10.1007/s12583-014-0455-1.

Darrouzet-Nardi, A., Reed, S.C., Grote, E.E., Belnap, J., 2018. Patterns of longer-term climate change effects on $CO_2$ efflux from biocrusted soils differ from those observed in the short term. Biogeosciences 15, 4561–4573. https://doi.org/10.5194/bg-15-4561-2018.

Davidson, G.R., Phillips-Housley, A., Stevens, M.T., 2013. Soil-zone adsorption of atmospheric CO2 as a terrestrial carbon sink. Geochim. Cosmochim. Acta 106, 44–50. https://doi.org/10.1016/j.gca.2012.12.015.

Dusza, Y., Sanchez-Cañete, E.P., Galliard, J.-F.L., Ferrière, R., Chollet, S., Massol, F., Hansart, A., Juarez, S., Dontsova, K., van Haren, J., Troch, P., Pavao-Zuckerman, M. A., Hamerlynck, E., Barron-Gafford, G.A., 2020. Biotic soil-plant interaction processes explain most of hysteretic soil CO2 efflux response to temperature in cross-factorial mesocosm experiment. Sci. Rep. 10, 905. https://doi.org/10.1038/s41598-019-55390-6.

Eldridge, D.J., Reed, S., Travers, S.K., Bowker, M.A., Maestre, F.T., Ding, J., Havrilla, C., Rodriguez-Caballero, E., Barger, N., Weber, B., Antoninka, A., Belnap, J., Chaudhary, B., Faist, A., Ferrenberg, S., Huber-Sannwald, E., Malam Issa, O., Zhao, Y., 2020. The pervasive and multifaceted influence of biocrusts on water in the world's drylands. Glob. Change Biol. 26, 6003–6014. https://doi.org/10.1111/gcb.15232.

Fa, K., Liu, J.-B., Zhang, Y.-Q., Wu, B., Qin, S.-G., Feng, W., Lai, Z.-R., 2015. CO2 absorption of sandy soil induced by rainfall pulses in a desert ecosystem. Hydrol. Process. 29, 2043–2051. https://doi.org/10.1002/hyp.10350.

Fa, K., Liu, Z., Zhang, Y., Qin, S., Wu, B., Liu, J., 2016a. Abiotic carbonate dissolution traps carbon in a semiarid desert. Sci. Rep. 6, 23570. https://doi.org/10.1038/srep23570.

Fa, K., Zhang, Y.-Q., Wu, B., Qin, S.-G., Liu, Z., She, W.-W., 2016b. Patterns and possible mechanisms of soil CO2 uptake in sandy soil. Sci. Total Environ. 544, 587–594. https://doi.org/10.1016/j.scitotenv.2015.11.163.

Gallagher, T.M., Breecker, D.O., 2020. The obscuring effects ofcalcite dissolution and formationon quantifying soil respiration. Glob. Biogeochem. Cycles 34 (12), e2020GB006584. https://doi.org/10.1029/2020GB006584.

Ganot, Y., Dragila, M.I., Weisbrod, N., 2014. Impact of thermal convection on CO2 flux across the earth–atmosphere boundary in high-permeability soils. Agric. For. Meteorol. 184, 12–24. https://doi.org/10.1016/j.agrformet.2013.09.001.

Gao, Y., Zhao, Z., Zhang, Y., Liu, J., 2021. Response of abiotic soil CO2 flux to the difference in air-soil temperature in a desert. Sci. Total Environ. 785, 147377 https://doi.org/10.1016/j.scitotenv.2021.147377.

Garcia-Pichel, F., 2023. The microbiology of biological soil crusts. Annu. Rev. Microbiol. 77 https://doi.org/10.1146/annurev-micro-032521-015202 annurev-micro-032521-015202.

Garcia-Pichel, F., Belnap, J., 1996. Microenvironments and microscale productivity of cyanobacterial desert Crusts1. J. Phycol. 32, 774–782. https://doi.org/10.1111/j.0022-3646.1996.00774.x.

Ghiloufi, W., Yun, J., Kim, J., Lee, J., Kang, H., 2023. The influences of lichens on soil physico-chemical properties, enzymes and microbes are species specific: insights from South Mediterranean arid ecosystem. Appl. Soil Ecol. 181, 104656 https://doi.org/10.1016/j.apsoil.2022.104656.

Goffin, S., Wylock, C., Haut, B., Maier, M., Longdoz, B., Aubinet, M., 2015. Modeling soil CO2 production and transport to investigate the intra-day variability of surface efflux and soil CO2 concentration measurements in a Scots Pine Forest (Pinus Sylvestris, L.). Plant and Soil 390, 195–211. https://doi.org/10.1007/s11104-015-2381-0.

Grünzweig, J.M., De Boeck, H.J., Rey, A., Santos, M.J., Adam, O., Bahn, M., Belnap, J., Deckmyn, G., Dekker, S.C., Flores, O., Gliksman, D., Helman, D., Hultine, K.R., Liu, L., Meron, E., Michael, Y., Sheffer, E., Throop, H.L., Tzuk, O., Yakir, D., 2022. Dryland mechanisms could widely control ecosystem functioning in a drier and warmer world. Nat. Ecol. Evol. 6, 1064–1076. https://doi.org/10.1038/s41559-022-01779-y.

Hamerlynck, E.P., Scott, R.L., Sánchez-Cañete, E.P., Barron-Gafford, G.A., 2013. Nocturnal soil CO2 uptake and its relationship to subsurface soil and ecosystem carbon fluxes in a Chihuahuan Desert shrubland. J. Geophys. Res. Biogeo. 118, 1593–1603. https://doi.org/10.1002/2013JG002495.

Houghton, R.A., Baccini, A., Walker, W.S., 2018. Where is the residual terrestrial carbon sink? Glob. Change Biol. 24, 3277–3279. https://doi.org/10.1111/gcb.14313.

Huang, W., Ertekin, E., Wang, T., Cruz, L., Dailey, M., DiRuggiero, J., Kisailus, D., 2020. Mechanism of water extraction from gypsum rock by desert colonizing microorganisms. Proc. Natl. Acad. Sci. 117, 10681–10687. https://doi.org/10.1073/pnas.2001613117.

IPCC, 2013. In: Stocker, T.F., Qin, D., Plattner, G.-K., Tignor, M., Allen, S.K., Boschung, J., Nauels, A., Xia, Y., Bex, V., Midgley, P.M. (Eds.), Climate Change 2013: The Physical Science Basis. Contribution of Working Group I to the Fifth Assessment Report of the Intergovern- mental Panel on Climate Change. Cambridge University Press, Cambridge, United Kingdom and New York, NY, USA, 1535–pp.

Jansson, C., Northen, T., 2010. Calcifying cyanobacteria—the potential of biomineralization for carbon capture and storage. Curr. Opin. Biotechnol., Energy biotechnology – Environmental biotechnology 21, 365–371. https://doi.org/10.1016/j.copbio.2010.03.017.

Jian, J., Bailey, V., Dorheim, K., Konings, A.G., Hao, D., Shiklomanov, A.N., Snyder, A., Steele, M., Teramoto, M., Vargas, R., Bond-Lamberty, B., 2022. Historically inconsistent productivity and respiration fluxes in the global terrestrial carbon cycle. Nat. Commun. 13, 1733. https://doi.org/10.1038/s41467-022-29391-5.

Jochheim, H., Wirth, S., Gartiser, V., Paulus, S., Haas, C., Gerke, H.H., Maier, M., 2022. Dynamics of soil CO2 efflux and vertical CO2 production in a european beech and a scots pine forest. Front. For. Glob. Change 5, 93. https://doi.org/10.3389/ffgc.2022.826298.

Kargas, G., Londra, P., Sgoubopoulou, A., 2020. Comparison of soil EC values from methods based on 1:1 and 1:5 soil to water ratios and ECe from saturated paste extract based method. Water 12, 1010. https://doi.org/10.3390/w12041010.

Kidron, G.J., Wang, Y., Herzberg, M., 2020. Exopolysaccharides may increase biocrust rigidity and induce runoff generation. J. Hydrol. 588, 125081 https://doi.org/10.1016/j.jhydrol.2020.125081.

Kim, M., 2024. The simplified field application of Desert Biocrust Model (sfDBM). In: Unravelling the main mechanism responsible for the nocturnal CO2 uptake by dryland soils. Zenodo. https://doi.org/10.5281/zenodo.10843357.

Kim, M., Or, D., 2017. Hydration status and diurnal trophic interactions shape microbial community function in desert biocrusts. Biogeosciences 14, 5403–5424. https://doi.org/10.5194/bg-14-5403-2017.

Kim, M., Or, D., 2019. Microscale pH variations during drying of soils and desert biocrusts affect HONO and NH 3 emissions. Nat. Commun. 10, 1–12. https://doi.org/10.1038/s41467-019-11956-6.

Kratz, A.M., Maier, S., Weber, J., Kim, M., Mele, G., Gargiulo, L., Leifke, A.L., Prass, M., Abed, R.M.M., Cheng, Y., Su, H., Pöschl, U., Weber, B., 2022. Reactive nitrogen hotspots related to microscale heterogeneity in biological soil crusts. Environ. Sci. Technol. 56, 11865–11877. https://doi.org/10.1021/acs.est.2c02207.

Lal, R., 2001. Potential of desertification control to sequester carbon and mitigate the greenhouse effect. Clim. Change 51, 35–72. https://doi.org/10.1023/A:1017529816140.

Lal, R., 2019. Carbon cycling in global drylands. Curr. Clim. Change Rep. 5, 221–232. https://doi.org/10.1007/s40641-019-00132-z.

Lázaro, R., Cantón, Y., Solé-Benet, A., Bevan, J., Alexander, R., Sancho, L.G., Puigdefábregas, J., 2008. The influence of competition between lichen colonization and erosion on the evolution of soil surfaces in the Tabernas badlands (SE Spain) and its landscape effects. Geomorphology 102, 252–266. https://doi.org/10.1016/j.geomorph.2008.05.005.

Li, C.H., Lee, C.K., 1993. Minimum cross entropy thresholding. Pattern Recogn. 26, 617–625. https://doi.org/10.1016/0031-3203(93)90115-D.
Liu, J., Fa, K., Zhang, Y., Wu, B., Qin, S., Jia, X., 2015. Abiotic CO2 uptake from the atmosphere by semiarid desert soil and its partitioning into soil phases. Geophys. Res. Lett. 42, 5779–5785. https://doi.org/10.1002/2015GL064689.
Liu, Z., Zhang, Y., Fa, K., Zhao, H., Qin, S., Yan, R., Wu, B., 2018. Desert soil bacteria deposit atmospheric carbon dioxide in carbonate precipitates. CATENA 170, 64–72. https://doi.org/10.1016/J.CATENA.2018.06.001.
Liu, Z., Sun, Yanfei, Zhang, Y., Qin, S., Sun, Yongqi, Mao, H., Miao, L., 2020. Desert soil sequesters atmospheric CO2 by microbial mineral formation. Geoderma 361, 114104. https://doi.org/10.1016/J.GEODERMA.2019.114104.
Lopez-Canfin, C., Lázaro, R., Sánchez-Cañete, E.P., 2022a. Water vapor adsorption by dry soils: a potential link between the water and carbon cycles. Sci. Total Environ. 824, 153746 https://doi.org/10.1016/j.scitotenv.2022.153746.
Lopez-Canfin, C., Lázaro, R., Sánchez-Cañete, E.P., 2022b. Disparate responses of soil-atmosphere CO2 exchange to biophysical and geochemical factors over a biocrust ecological succession in the Tabernas Desert. Geoderma 425, 116067. https://doi.org/10.1016/j.geoderma.2022.116067.
Lopez-Canfin, C., Sánchez-Cañete, E.P., Lázaro, R., 2024. Hourly time series of soil and atmosphere variables at the experimental site of El Cautivo, Tabernas Desert, Almeria, Spain (February 2018 to December 2019) [Data set]. Zenodo. https://doi.org/10.5281/zenodo.10836173.
Lu, H., Li, S., Ma, M., Bastrikov, V., Chen, X., Ciais, P., Dai, Y., Ito, A., Ju, W., Lienert, S., Lombardozzi, D., Lu, X., Maignan, F., Nakhavali, M., Quine, T., Schindlbacher, A., Wang, J., Wang, Y., W rlind, D., Zhang, S., Yuan, W., 2021. Comparing machine learning-derived global estimates of soil respiration and its components with those from terrestrial ecosystem models. Environ. Res. Lett. 16, 54048. https://doi.org/10.1088/1748-9326/ABF526.
Ma, J., Wang, Z.-Y., Stevenson, B.A., Zheng, X.-J., Li, Y., 2013. An inorganic CO2 diffusion and dissolution process explains negative CO2 fluxes in saline/alkaline soils. Sci. Rep. 3, 2025. https://doi.org/10.1038/srep02025.
Ma, J., Liu, R., Tang, L.-S., Lan, Z.-D., Li, Y., 2014. A downward $CO_2$ flux seems to have nowhere to go. Biogeosciences 11, 6251–6262. https://doi.org/10.5194/bg-11-6251-2014.
Miralles, I., Ladrón de Guevara, M., Chamizo, S., Rodríguez-Caballero, E., Ortega, R., van Wesemael, B., Cantón, Y., 2018. Soil CO2 exchange controlled by the interaction of biocrust successional stage and environmental variables in two semiarid ecosystems. Soil Biol. Biochem. 124, 11–23. https://doi.org/10.1016/j.soilbio.2018.05.020.
Miralles, I., Lázaro, R., Sánchez-Marañón, M., Soriano, M., Ortega, R., 2020. Biocrust cover and successional stages influence soil bacterial composition and diversity in semiarid ecosystems. Sci. Total Environ. 709, 134654 https://doi.org/10.1016/j.scitotenv.2019.134654.
Miralles-Mellado, I., Cantón, Y., Solé-Benet, A., 2011. Two-dimensional porosity of crusted silty soils: indicators of soil quality in semiarid rangelands? Soil Sci. Soc. Am. J. 75, 1330–1342. https://doi.org/10.2136/sssaj2010.0283.
Monger, H.C., Kraimer, R.A., Khresat, S., Cole, D.R., Wang, X., Wang, J., 2015. Sequestration of inorganic carbon in soil and groundwater. Geology 43, 375–378. https://doi.org/10.1130/G36449.1.
Ortiz, A.C., Jin, L., Ogrinc, N., et al., 2022. Dryland irrigation increases accumulation rates of pedogenic carbonate and releases soil abiotic $CO_2$. Sci. Rep. 12, 464. https://doi.org/10.1038/s41598-021-04226-3.
Phillips, C.L., Nickerson, N., Risk, D., Bond, B.J., 2011. Interpreting diel hysteresis between soil respiration and temperature. Glob. Change Biol. 17, 515–527. https://doi.org/10.1111/j.1365-2486.2010.02250.x.
Plaza, C., Zaccone, C., Sawicka, K., Méndez, A.M., Tarquis, A., Gascó, G., Heuvelink, G.B. M., Schuur, E.A.G., Maestre, F.T., 2018. Soil resources and element stocks in drylands to face global issues. Sci. Rep. https://doi.org/10.1038/s41598-018-32229-0, 2018 81 8, 1–8.
Pumpanen, J., Ilvesniemi, H., Hari, P., 2003. A process-based model for predicting soil carbon dioxide efflux and concentration. Soil Sci. Soc. Am. J. 67, 402–413. https://doi.org/10.2136/sssaj2003.4020.
Richardson, D.H., 2002. Reflections on lichenology: achievements over the last 40 years and challenges for the future. Can. J. Bot. 80, 101–113. https://doi.org/10.1139/b02-011.
Riveros-Iregui, D.A., Emanuel, R.E., Muth, D.J., McGlynn, B.L., Epstein, H.E., Welsch, D. L., Pacific, V.J., Wraith, J.M., 2007. Diurnal hysteresis between soil CO $_2$ and soil temperature is controlled by soil water content. Geophys. Res. Lett. 34, L17404. https://doi.org/10.1029/2007GL030938.
Roland, M., Serrano-Ortiz, P., Kowalski, A.S., Goddéris, Y., Sánchez-Cañete, E.P., Ciais, P., Domingo, F., Cuezva, S., Sanchez-Moral, S., Longdoz, B., Yakir, D., Van Grieken, R., Schott, J., Cardell, C., Janssens, I.A., 2013. Atmospheric turbulence triggers pronounced diel pattern in karst carbonate geochemistry. Biogeosciences 10, 5009–5017. https://doi.org/10.5194/bg-10-5009-2013.
Ryan, M.G., Law, B.E., 2005. Interpreting, measuring, and modeling soil respiration. Biogeochemistry 73, 3–27. https://doi.org/10.1007/s10533-004-5167-7.
Sagi, N., Zaguri, M., Hawlena, D., 2021. Soil CO2 influx in drylands: a conceptual framework and empirical examination. Soil Biol. Biochem. 156, 108209 https://doi.org/10.1016/J.SOILBIO.2021.108209.
Sánchez-Cañete, E.P., Scott, R.L., van Haren, J., Barron-Gafford, G.A., 2017. Improving the accuracy of the gradientmethod for determining soil carbondioxide efflux. J. Geophys. Res. Biogeosci. 122, 50–64. https://doi.org/10.1002/2016JG003530.
Sánchez-Cañete, E.P., Barron-Gafford, G.A., Chorover, J., 2018. A considerable fraction of soil-respired CO2 is not emitted directly to the atmosphere. Sci. Rep. 8, 13518. https://doi.org/10.1038/s41598-018-29803-x.
Sander, R., 2015. Compilation of Henry's law constants (version 4.0) for water as solvent. Atmospheric Chem. Phys. 15, 4399–4981. https://doi.org/10.5194/acp-15-4399-2015.
Sanderman, J., 2012. Can management induced changes in the carbonate system drive soil carbon sequestration? A review with particular focus on Australia. Agric. Ecosyst. Environ. 155, 70–77. https://doi.org/10.1016/j.agee.2012.04.015.
Schlesinger, W.H., 2017. An evaluation of abiotic carbon sinks in deserts. Glob. Change Biol. 23, 25–27. https://doi.org/10.1111/gcb.13336.
Schlesinger, W.H., Belnap, J., Marion, G., 2009. On carbon sequestration in desert ecosystems. Glob. Change Biol. 15, 1488–1490. https://doi.org/10.1111/j.1365-2486.2008.01763.x.
Šimůnek, J., Suarez, D.L., 1993. Modeling of carbon dioxide transport and production in soil: 1. Model development. Water Resour. Res. 29, 487–497. https://doi.org/10.1029/92WR02225.
Song, W., Chen, S., Zhou, Y., Wu, B., Zhu, Y., Lu, Q., Lin, G., 2015. Contrasting diel hysteresis between soil autotrophic and heterotrophic respiration in a desert ecosystem under different rainfall scenarios. Sci. Rep. 5, 16779. https://doi.org/10.1038/srep16779.
Soper, F.M., McCalley, C.K., Sparks, K., Sparks, J.P., 2017. Soil carbondioxide emissions from the Mojavedesert: isotopic evidence for a carbo-nate source. Geophys. Res. Lett. 44, 245–251. https://doi.org/10.1002/2016GL071198.
Souza-Egipsy, V., Wierzchos, J., Sancho, C., Belmonte, A., Ascaso, C., 2004. Role of biological soil crust cover in bioweathering and protection of sandstones in a semi-arid landscape (Torrollones de Gabarda, Huesca, Spain). Earth Surf. Process. Landf. 29, 1651–1661. https://doi.org/10.1002/esp.1118.
Spohn, M., Holzheu, S., 2021. Temperature controls diel oscillation of the CO2 concentration in a desert soil. Biogeochemistry 156, 279–292. https://doi.org/10.1007/s10533-021-00845-0.
Spohn, M., Müller, K., Höschen, C., Mueller, C.W., Marhan, S., 2020. Dark microbial CO2 fixation in temperate forest soils increases with CO2 concentration. Glob. Change Biol. 26, 1926–1935. https://doi.org/10.1111/gcb.14937.
Stekhoven, D.J., Bühlmann, P., 2012. MissForest—non-parametric missing value imputation for mixed-type data. Bioinforma. Oxf. Engl. 28, 112–118. https://doi.org/10.1093/bioinformatics/btr597.
Sun, F., Xiao, B., Kidron, G.J., Heitman, J.L., 2022. Insights about biocrust effects on soil gas transport and aeration in drylands: permeability, diffusivity, and their connection to hydraulic conductivity. Geoderma 427, 116137. https://doi.org/10.1016/j.geoderma.2022.116137.
Sun, F., Xiao, B., Li, S., Yu, X., Kidron, G.J., Heitman, J., 2023. Direct evidence and mechanism for biocrusts-induced improvements in pore structure of dryland soil and the hydrological implications. J. Hydrol. 623, 129846 https://doi.org/10.1016/j.jhydrol.2023.129846.
Tamm, A., Caesar, J., Kunz, N., Colesie, C., Reichenberger, H., Weber, B., 2018. Ecophysiological properties of three biological soil crust types and their photoautotrophs from the Succulent Karoo, South Africa. Plant and Soil 429, 127–146. https://doi.org/10.1007/s11104-018-3635-4.
Taylor, L.L., Beerling, D.J., Quegan, S., Banwart, S.A., 2017. Simulating carbon capture by enhanced weathering with croplands: an overview of key processes highlighting areas of future model development. Biol. Lett. 13, 20160868. https://doi.org/10.1098/rsbl.2016.0868.
Tuller, M., Or, D., Dudley, L.M., 1999. Adsorption and capillary condensation in porous media: liquid retention and interfacial configurations in angular pores. Water Resour. Res. 35, 1949–1964. https://doi.org/10.1029/1999WR900098.
Wang, J., Monger, C., Wang, X., Serena, M., Leinauer, B., 2016. Carbon sequestration in response to Grassland–Shrubland–Turfgrass conversions and a test for carbonate biomineralization in desert soils, New mexico, USA. Soil Sci. Soc. Am. J. 80, 1591–1603. https://doi.org/10.2136/SSSAJ2016.03.0061.
Wang, L., Kaseke, K.F., Seely, M.K., 2017. Effects of non-rainfall water inputs on ecosystem functions. WIREs Water 4, e1179. https://doi.org/10.1002/wat2.1179.
Wang, Z.-Y., Xie, J.-B., Wang, Y.-G., Li, Y., 2020. Biotic and abiotic contribution to diurnal soil CO2 fluxes from saline/alkaline soils. Sci. Rep. 10, 5396. https://doi.org/10.1038/s41598-020-62209-2.
Waring, B.G., Powers, J.S., 2016. Unraveling the mechanisms underlying pulse dynamics of soil respiration in tropical dry forests. Environ. Res. Lett. 11, 105005 https://doi.org/10.1088/1748-9326/11/10/105005.
Weber, B., Tamm, A., Maier, S., Rodríguez-Caballero, E., 2018. Biological soil crusts of the Succulent Karoo: a review§. Afr. J. Range Forage Sci. 35, 335–350. https://doi.org/10.2989/10220119.2018.1527782.
Weber, B., Belnap, J., Büdel, B., Antoninka, A.J., Barger, N.N., Chaudhary, V.B., Darrouzet-Nardi, A., Eldridge, D.J., Faist, A.M., Ferrenberg, S., Havrilla, C.A., Huber-Sannwald, E., Malam Issa, O., Maestre, F.T., Reed, S.C., Rodriguez-Caballero, E., Tucker, C., Young, K.E., Zhang, Y., Zhao, Y., Zhou, X., Bowker, M.A., 2022. What is a biocrust? A refined, contemporary definition for a broadening research community. Biol. Rev. 97, 1768–1785. https://doi.org/10.1111/brv.12862.
Wu, Y., Rao, B., Wu, P., Liu, Y., Li, G., Li, D., 2013. Development of artificially induced biological soil crusts in fields and their effects on top soil. Plant and Soil 370, 115–124. https://doi.org/10.1007/s11104-013-1611-6.
Yang, F., Huang, J., He, Q., Zheng, X., Zhou, C., Pan, H., Huo, W., Yu, H., Liu, X., Meng, L., Han, D., Ali, M., Yang, X., 2020. Impact of differences in soil temperature on the desert carbon sink. Geoderma 379, 114636. https://doi.org/10.1016/J.GEODERMA.2020.114636.
Yates, E.L., Detweiler, A.M., Iraci, L.T., Bebout, B.M., McKay, C.P., Schiro, K., Sheffner, E. J., Kelley, C.A., Tadić, J.M., Loewenstein, M., 2013. Assessing the role of alkaline

soils on the carbon cycle at a playa site. Environ. Earth Sci. 70, 1047–1056. https://doi.org/10.1007/s12665-012-2194-x.

Yu, L., Daniels, L.M., Mulders, J.J.P.A., Saldi, G.D., Harrison, A.L., Liu, L., Oelkers, E.H., 2019. An experimental study of gypsum dissolution coupled to CaCO3 precipitation and its application to carbon storage. Chem. Geol. 525, 447–461. https://doi.org/10.1016/J.CHEMGEO.2019.08.005.

Zhang, Q., Katul, G.G., Oren, R., Daly, E., Manzoni, S., Yang, D., 2015. The hysteresis response of soil CO2 concentration and soil respiration to soil temperature. J. Geophys. Res. Biogeo. 120, 1605–1618. https://doi.org/10.1002/2015JG003047.